PHILOSOPHICAL TRANSACTIONS OF THE ROYAL SOCIETY A MATHEMATICAL, PHYSICAL & ENGINEERING SCIENCES

The Weighted Average Flux Method Applied to the Euler Equations

E. F. Toro

Phil. Trans. R. Soc. Lond. A 1992 **341**, 499-530
doi: 10.1098/rsta.1992.0113

The weighted average flux method applied to the Euler equations

By E. F. Toro

Department of Aerodynamics and Fluid Mechanics, College of Aeronautics, Cranfield Institute of Technology, Cranfield, Bedfordshire MK43 0AL, U.K.

Contents

The weighted average flux method (WAF) for general hyperbolic conservation laws was formulated by Toro. Here the method is specialized to the time-dependent Euler equations of gas dynamics. Several improvements to the technique are presented. These have resulted from experience obtained from applying WAF to a variety of realistic problems. A hierarchy of solutions to the relevant Riemann problem, ranging from very simple approximations to the exact solution, are presented. Their performance in the WAF method for several test problems in one and two dimensions is assessed.

1. Introduction

A significant contribution to the current state of modern computational fluid dynamics (CFD) has come via Riemann-problem based, or Godunov-type, numerical

Phil. Trans. R. Soc. Lond. A (1992) **341**, 499–530
Printed in Great Britain

methods. These are extensions of the first-order accurate method of Godunov (1959). Riemann-problem based methods (or RP methods for short) are directly applicable to time-dependent one-dimensional systems of hyperbolic conservation laws or to two-dimensional systems that are hyperbolic in a time-like variable (e.g. the two-dimensional steady supersonic Euler equations). Extensions of these methods to multi-dimensional problems is carried out via the finite volume method coupled with one-dimensional physics in the direction normal to the control volume interface.

Many workers have contributed to the development of RP methods; outstanding examples are Godunov (1959), van Leer (1979), Roe (1981), Harten (1983), Osher (1984).

RP methods use the solution of the Riemann problem with data in volumes $(i, i+1)$ to define an intercell numerical flux $F_{i+\frac{1}{2}}$ to be used in the conservative, explicit formula

$$U_i^{n+1} = U_i^n - (\Delta t/\Delta x)\,(F_{i-\frac{1}{2}} - F_{i+\frac{1}{2}}).$$

The various RP methods differ in the definition for the intercell flux $F_{i+\frac{1}{2}}$, in the way the local Riemann problem solution is used and in the way higher accuracy without the spurious oscillations of traditional methods is achieved.

The weighted average flux (WAF) approach for systems of hyperbolic conservation laws was presented by Toro (1989*a*). This method achieves second-order accuracy by using the conventional piecewise constant data Riemann problem. Also, it is sufficiently flexible to accept virtually any approximation to the solution of the local Riemann problem as well as the exact solution. This second feature can be taken advantage of by constructing a hierarchy of Riemann solvers to be used in an adaptive Riemann solver fashion.

The WAF method has been applied to a variety of realistic flow situations (Toro 1989*b*, 1991, 1992). The experience gained in the exercise has resulted in further developments and useful simplifications to the technique. In this paper we present the method as applied specifically to the time-dependent Euler equations in one and two space dimensions. An efficient exact Riemann solver as well as a variety of approximate Riemann solvers that can be used with WAF are presented.

The paper is organized as follows. In §2 the method is presented in its current formulation; §3 deals with Riemann solvers; in §4 we present the construction of the oscillation-free version of the method. Some numerical results are presented in §5 and conclusions are drawn in §6.

2. Formulations of the WAF method

For the purpose of this section we shall restrict ourselves to the time-dependent one-dimensional Euler equations written in conservation form, namely

$$U_t + [F(U)]_x = 0. \tag{1}$$

Here U is the vector of conserved variables and $F(U)$ is the vector of the corresponding fluxes, i.e.

$$U = \begin{bmatrix} \rho \\ \rho u \\ E \end{bmatrix}, \quad F = \begin{bmatrix} \rho u \\ \rho u^2 + p \\ u(E+p) \end{bmatrix}. \tag{2}$$

Figure 1

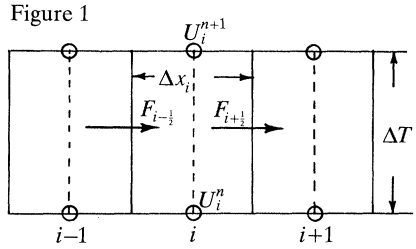

Figure 2

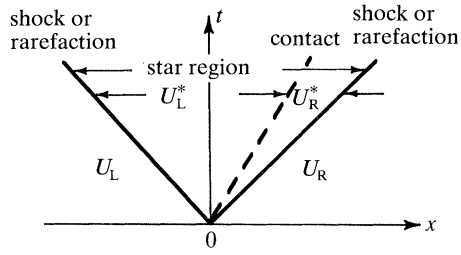

Figure 1. Control volume of dimensions Δx_i by Δt is computational cell i. New value U_i^{n+1} is given in terms of old value U_i^n and intercell fluxes.

Figure 2. Solution of the Riemann problem with data U_L and U_R in the xt-plane. The three waves present define four piecewise constant states. Solution is found in terms of the star region between acoustic waves.

The conserved variables are: the density ρ, the momentum ρu, where u is the velocity, and the total energy E, where $E = \frac{1}{2}\rho u^2 + \rho e$ with e denoting the specific internal, or intrinsic, energy.

The symbols t and x denote time and space and are the independent variables. The associated subscripts in (1) denote partial differentiation. Note that there are more dependent variables than there are equations and thus a closure condition is required. We take the ideal gas equation of state as the closure condition, namely

$$e = e(\rho, p) = p/(\gamma - 1)\rho \tag{3}$$

with γ denoting ratio of specific heats.

The Euler equations have discontinuous solutions (shock waves, contacts) and it is therefore more appropriate to recast the differential equations (1) in integral form as

$$\oint [U\,\mathrm{d}x - F(U)\,\mathrm{d}t] = 0. \tag{4}$$

Consider a domain in the xt-plane discretized by a grid of dimensions Δx_i and Δt as shown in figure 1. Evaluation of the integral (4) around cell i produces

$$U_i^{n+1} = U_i^n - (\Delta t/\Delta x_i)\,[F_{i+\frac{1}{2}} - F_{i-\frac{1}{2}}] \tag{5}$$

with suitable interpretations for the discrete values of the conserved variables and fluxes. This explicit conservative formula gives a time-marching scheme in terms of the data U_i^n, the grid dimensions and the intercell fluxes $F_{i+\frac{1}{2}}$ and $F_{i-\frac{1}{2}}$. The notation U_i^n means the discrete value of U in cell i at time level n. For convenience, we often omit the superscript n.

The scheme (5) is completely defined once the fluxes have been specified. Let us consider $F_{i+\frac{1}{2}}$. The WAF method assumes that all conserved variables have a piecewise constant distribution in x at any time level n. Locally, two neighbouring constant states (U_i, U_{i+1}) are the initial data for the relevant differential (or integral) equations. This initial value problem is known as the *Riemann problem*. In general, this local problem is simpler to solve than the global problem. The global solution can be constructed by using the sequence of local Riemann problems $\{RP(i, i+1)\}$ in a variety of ways, depending on the particular method in use. The solution of the

PHILOSOPHICAL TRANSACTIONS OF THE ROYAL SOCIETY A MATHEMATICAL, PHYSICAL & ENGINEERING SCIENCES

Riemann problem for the unsteady one-dimensional Euler equations (1), when represented on the xt-plane, looks as depicted in figure 2. There are three waves. The middle wave is always a contact discontinuity. The left and right waves are called the acoustic waves and can be either shocks or rarefactions. Contacts and shocks are discontinuities, rarefaction waves are continuous solutions. We shall denote the solution of the Riemann problem with data U_i and U_{i+1} by $U^*(x/t, U_i, U_{i+1})$ or simply by $U^*(x/t)$. It is only a function of the similarity variable x/t. Note that we centre the Riemann problem at the origin $(0, 0)$ in the xt-plane.

Godunov (1959) is credited with being the first to use the solution of the local Riemann problems to evaluate the numerical intercell flux $F_{i+\frac{1}{2}}$ in (5). Godunov's flux is given by

$$F^{\mathrm{GOD}}_{i+\frac{1}{2}} = F[U^*(0, U_i, U_{i+1})]. \tag{6}$$

Note that $U^*(0, U_i, U_{i+1})$ is constant for $t > 0$. The density (and thus the internal energy and the temperature) is constant in between the waves with discontinuous jumps across shocks and contacts. The structure of the solution of the Riemann problem contains therefore four constant states: U_i (left state data), U^*_{L} (left of contact), U^*_{R} (right of contact) and U_{i+1} (right state data). Special care is needed in the case when the value $x/t = 0$ lies inside a rarefaction fan (sonic flow). The Godunov method is only first-order accurate and is therefore too inaccurate to be used in practice.

The WAF method (Toro 1989*a*) is a second-order extension of Godunov's method. Higher accuracy is achieved by simply defining the intercell flux $F_{i+\frac{1}{2}}$ as an integral average of the flux function $F(U)$ in (1) evaluated at the solution $U^*(x/t)$ of the Riemann problem with data U_i, U_{i+1} at time $t = \frac{1}{2}\Delta t$.

Suppose the neighbouring cells i and $i+1$ have spacings Δx_i and Δx_{i+1}, then the WAF flux is

$$\left.\begin{aligned} F^{\mathrm{WAF}}_{i+\frac{1}{2}} &= \frac{1}{2x_1}\int_{x_1}^{0} F(U^*)\,\mathrm{d}x + \frac{1}{2x_2}\int_{0}^{x_2} F(U^*)\,\mathrm{d}x, \\ x_1 &= -\tfrac{1}{2}\Delta x_i; \quad x_2 = \tfrac{1}{2}\Delta x_{i+1}, \end{aligned}\right\} \tag{7}$$

where $U^* = U(x/\frac{1}{2}\Delta t)$ is the solution of the Riemann problem with data U^n_i, U^n_{i+1} at time $\frac{1}{2}\Delta t$. The integration in (7) goes from the centre of the left cell i to the centre of the right cell $i+1$ at time $t = \frac{1}{2}\Delta t = \text{const}$. A simpler expression results by choosing

$$x_1 = -\tfrac{1}{2}\min(\Delta x_i, \Delta x_{i+1}), \quad x_2 = \tfrac{1}{2}\min(\Delta x_i, \Delta x_{i+1}).$$

The integration can be made as accurate as desired, but the presence of rarefaction fans makes it more complicated, which for practical applications is undesirable. Experience has indicated to us that acknowledging fans is only important in the presence of sonic flow, that is, when one of the acoustic waves is a rarefaction centred around the t-axis, and even in this case one may simplify the wave structure, as we shall explain later. In any event, we assume that the solution of the Riemann problem has N waves with N associated wave speeds λ_k. For simplicity let us consider the regular grid case with $\Delta x_i = \Delta x_{i+1} = \Delta x$. The Courant numbers ν_k associated with the wave speeds λ_k are

$$\nu_k = \lambda_k/(\Delta x/\Delta t). \tag{8}$$

PHILOSOPHICAL TRANSACTIONS OF THE ROYAL SOCIETY A MATHEMATICAL, PHYSICAL & ENGINEERING SCIENCES

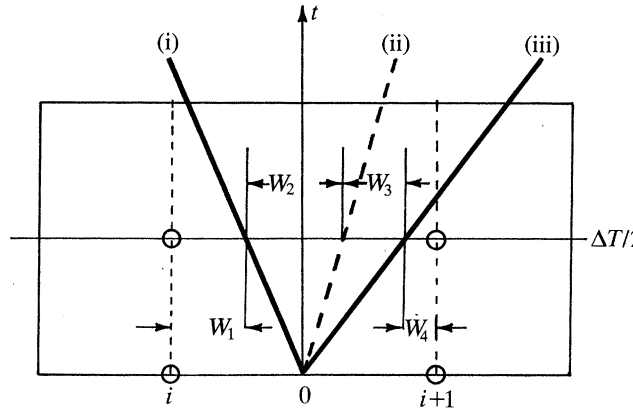

Figure 3. Evaluation of the intercell numerical flux for the WAF method. The simplified wave structure in the solution of the Riemann problem gives four regions k of non-dimensional length W_k. (i) $\mathrm{d}x/\mathrm{d}t = \lambda_1$; (ii) $\mathrm{d}x/\mathrm{d}t = \lambda_2 = u^*$; (iii) $\mathrm{d}x/\mathrm{d}t = \lambda_3$.

The WAF flux can then be written as

$$F_{i+\frac{1}{2}} = \sum_{k=1}^{N+1} W_k F_{i+\frac{1}{2}}^{(k)}, \tag{9}$$

where the coefficients W_k (or weights) are the geometric extents of the constant states in the integral (7). $F_{i+\frac{1}{2}}^{(k)}$ is the flux function F in (1) evaluated at the solution of the Riemann problem in region k. Figure 3 illustrates the situation. It is easy to see that the weights W_k can be written in terms of the Courant numbers ν_k as follows

$$W_k = \tfrac{1}{2}(\nu_k - \nu_{k-1}), \quad \nu_0 = -1 \quad \text{and} \quad \nu_{N+1} = 1. \tag{10}$$

Note that $W_k \geqslant 0$ for all k and that $\Sigma_{k=1}^{N+1} W_k = 1$.

Clearly $F_{i+\frac{1}{2}}^{\mathrm{WAF}}$ gives an extension of the first-order Godunov method, for if $W_K = 1$ and $W_k = 0$ for all $k \neq K$ in (9) $F_{i+\frac{1}{2}}^{\mathrm{WAF}}$ reproduces the Godunov flux. The region K is that associated with $x/t = 0$. The wave structure of the local Riemann problem $RP(i, i+1)$ determines which weight corresponds to the Godunov's method. For instance, if the flow is fully supersonic, i.e. $\lambda_1 > 0$ then W_1 is the Godunov's weight. If $\lambda_3 < 0$, then the Godunov's weight is W_4, etc. The case of t-axis centred expansion fans will be dealt with later when discussing solutions of the Riemann problem.

The Godunov's weight represents the upwind bias of the WAF scheme and controls stability. All other weights represent downwind contributions; they increase accuracy. When applied to the model hyperbolic equation

$$u_t + a u_x = 0, \quad a = \text{const.} \tag{11}$$

the WAF method reduces identically to the Lax–Wendroff method and it is therefore, for this model equation, second-order accurate in space and time. For nonlinear hyperbolic systems the numerical results are like those obtained by typical second-order accurate methods.

A disadvantage of the added accuracy of the WAF scheme is that spurious oscillations near high gradients are produced. This is in accordance with the well-

PHILOSOPHICAL TRANSACTIONS OF THE ROYAL SOCIETY A MATHEMATICAL, PHYSICAL & ENGINEERING SCIENCES

known Godunov's theorem (Godunov 1959). An oscillation free version of the method will be presented in §4. This is different from that given in the original paper (Toro 1989*a*) and simpler to implement in practice.

The WAF flux can be expressed, after using (10) in (9), as

$$F^{\mathrm{WAF}}_{i+\frac{1}{2}} = \tfrac{1}{2}[F_i + F_{i+1}] - \frac{1}{2}\sum_{k=1}^{N} \nu_k \, \Delta F^{(k)}_{i+\frac{1}{2}}, \tag{12}$$

where

$$\Delta F^{(k)}_{i+\frac{1}{2}} = F^{(k+1)}_{i+\frac{1}{2}} - F^{(k)}_{i+\frac{1}{2}} \tag{13}$$

is the flux jump across wave k.

Formulae (12) and (13) are more revealing. In particular, they expose the flux-difference splitting character of the method. Also, expression (12) makes is easier to compare the similarities and differences of the WAF method with those of other modern methods, such as Roe's method (Roe 1981).

An alternative formulation of the WAF method is

$$F^{\mathrm{WAF}}_{i+\frac{1}{2}} = F(\bar{V}_{i+\frac{1}{2}}), \tag{14}$$

where $\bar{V}_{i+\frac{1}{2}}$ is obtained by replacing the flux F in (9) by an actual state V. There are at least two choices for V, namely the vector of primitive variables (ρ, u, p) or the vector of conserved variables $(\rho, \rho u, E)$. In either case the average state can be written as

$$\bar{V}_{i+\frac{1}{2}} = \tfrac{1}{2}[V_i + V_{i+1}] - \frac{1}{2}\sum_{k=1}^{N} \nu_k \, \Delta V^{(k)}_{i+\frac{1}{2}}, \tag{15}$$

where

$$\Delta V^{(k)}_{i+\frac{1}{2}} = V^{(k+1)}_{i+\frac{1}{2}} - V^{(k)}_{i+\frac{1}{2}} \tag{16}$$

is the jump in V across the wave k and $V^{(k)}_{i+\frac{1}{2}}$ is the value of V in region k.

From the point of view of computational efficiency, formulae (14)–(16) are more attractive than (12) and (13); there are fewer operations involved. Numerical experiments show that the results of these two formulations are virtually indistinguishable. The same remark applies to the choice of variables for the states V in (14)–(16). From a theoretical point of view it is of interest to note that if the state V in (15) represents the conserved variables then this formulation of the WAF method makes it analogous to the Richtmyer–Morton method (Richtmyer & Morton 1967), where

$$\bar{V}_{i+\frac{1}{2}} = \tfrac{1}{2}[V_i + V_{i+1}] - \tfrac{1}{2}(\Delta t/\Delta x)\,[F_{i+1} - F_i]. \tag{17}$$

This can be immediately seen by integrating the conservation laws (1), or (4), in the rectangle

$$-\tfrac{1}{2}\Delta x \leqslant x \leqslant \tfrac{1}{2}\Delta x, \quad 0 \leqslant t \leqslant \tfrac{1}{2}\Delta t.$$

The Richtmyer–Morton method is also known as the two-step Lax–Wendroff method. For linear problems these two methods are identical. Thus version (14)–(16) of WAF is formally identical to the Lax–Wendroff method, for linear problems, when the vector V stands for conserved variables.

These traditional finite difference methods of Richtmyer & Morton and Lax–Wendroff make no reference to the solution of the local Riemann problem. It is this extra local information contained in the WAF method that will permit us to modify it so as to retain second-order accuracy in smooth parts of the flow and produce high resolution of discontinuities without spurious oscillations.

As a point of interest it is worth remarking that formulation (15) and (16) of WAF,

under certain special circumstances, may lead to entropy violating solutions (rarefaction shocks). This depends entirely on the solution of the Riemann problem.

3. Riemann solvers

To apply the WAF method to the Euler equations (1) the solution of the associated Riemann problem must be found. As seen in formulae (12) and (13), or (14)–(16), for the intercell flux $F_{i+\frac{1}{2}}$ we require (i) the wave speeds λ_k (to compute the Courant numbers ν_k) and (ii) the flux jumps, if (12) is used, or the state jumps, if (15) is used, across the waves.

The exact solution of the Riemann problem is capable of producing all of this information, accurately. Alternatively, one may use suitable approximations to the exact solution. More attractive still, one may select exact or approximate values depending on the local features of the flow. Near strong shocks for instance, where approximations to the solution of the Riemann problem are bound to cause difficulties, one can use the exact solution. Elsewhere one could use approximate solutions. For ideal gases, the extra computing cost involved in finding the exact solutions is not significant. Exact solvers have become very efficient (Toro 1987). These statements also hold for covolume gases (Toro 1989*c*). As to approximate Riemann solvers there are several in current use in the literature. They all have advantages and disadvantages and it is not possible to select a single one as the universal Riemann solver. An attractive feature of the present numerical method is the flexibility available when selecting the Riemann-problem solution.

(*a*) *The exact solution of the Riemann problem*

For ideal gases there are some very efficient exact Riemann solvers available. An interesting survey was carried out by Gottlieb & Groth (1988), who also reported on their own new solver.

Here we present a brief description of the ideal-gas version (Toro 1987) of an efficient exact Riemann solver for covolume gases (Toro 1989*c*). We briefly summarize the main steps in finding the solution. We first note that both the pressure p^* and velocity u^* between the acoustic waves (see figure 2) are constant. Then the main step is to derive a single algebraic (nonlinear) equation for either the velocity u^* or the pressure p^*. A point concerning notation, we shall often use V_{L} and V_{R} instead of V_i and V_{i+1}, where V is a vector representing an appropriate set of variables such as the conserved variables.

Following Toro (1987) we can write

$$f(p^*, V_{\mathrm{L}}, V_{\mathrm{R}}) \equiv f_{\mathrm{L}}(p^*, V_{\mathrm{L}}) + f_{\mathrm{R}}(p^*, V_{\mathrm{R}}) + u_{\mathrm{R}} - u_{\mathrm{L}} = 0, \tag{18}$$

where the functions f_{L} and f_{R} are derived from relations across the acoustic waves on the left and right. They depend on (i) the unknown pressure p^* (ii) the data (V_{L} or V_{R}) and (iii) the type of the acoustic wave (either shock or rarefaction). These functions are found to be

$$f_{\mathrm{L}} = \begin{cases} (H_{\mathrm{L}} - 1)\{2p_{\mathrm{L}}/\rho_{\mathrm{L}}[(\gamma+1)H_{\mathrm{L}} + \gamma - 1]\}^{\frac{1}{2}}, & \text{if} \quad H_{\mathrm{L}} > 1 \text{ (shock)}, \\ (2a_{\mathrm{L}}/(\gamma-1))[H_{\mathrm{L}}^m - 1], & \text{if} \quad H_{\mathrm{L}} \leqslant 1 \text{ (rarefaction)}, \end{cases} \tag{19}$$

$$f_{\mathrm{R}} = \begin{cases} (H_{\mathrm{R}} - 1)\{2p_{\mathrm{R}}/(\rho_{\mathrm{R}}[(\gamma+1)H_{\mathrm{R}} + \gamma - 1]\}^{\frac{1}{2}}, & \text{if} \quad H_{\mathrm{R}} > 1 \text{ (shock)}, \\ (2a_{\mathrm{R}}/(\gamma-1))[H_{\mathrm{R}}^m - 1], & \text{if} \quad H_{\mathrm{R}} \leqslant 1 \text{ (rarefaction)}, \end{cases} \tag{20}$$

PHILOSOPHICAL TRANSACTIONS OF THE ROYAL SOCIETY A MATHEMATICAL, PHYSICAL & ENGINEERING SCIENCES

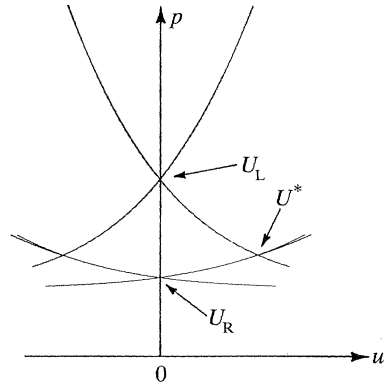

Figure 4. Rarefaction (dashed line) and shock (full line) curves in the up-plane for two data states U_L and U_R. Solution of Riemann problem in the star region is given by U^*.

where $$H_L = p^*/p_L, \quad H_R = p^*/p_R, \quad m = (\gamma-1)/2\gamma \tag{21}$$

and a_L, a_R denote the sound speed on the left and right states respectively. As f in (18) is monotone, a unique solution for physically admissible data exists, and thus a Newton–Raphson iteration procedure for (18) to find p^* works well, particularly if a good initial guess is used. If in (19)–(21) one chooses the rarefaction branches the following closed-form solution for p^* is obtained, namely

$$p_0^* = \left[\frac{a_L + a_R + (u_L - u_R)(\gamma-1)/2}{a_L/p_L^m + a_R/p_R^m}\right]^{1/m}. \tag{22}$$

For most of a typical flow domain this is a very accurate approximation. Figure 4 shows a comparison between the exact value and the approximation (22) for p^*. It can be seen that for pressure ratios H_L, H_R below 4 the difference is almost negligible. In any event, p_0^* is a good guess for an iteration procedure. For very strong shocks a converged exact solution is achieved in about three iterations. Once p^* has been found u^* follows as

$$u^* = u_R + f_R, \quad \text{or} \quad u^* = u_L - f_L,$$

or a mean value.

$$u^* = \tfrac{1}{2}(u_L + u_R) + \tfrac{1}{2}(f_R - f_L). \tag{23}$$

The next step is to find the density values ρ_L^* and ρ_R^* either side of the contact discontinuity. These again depend on the type of acoustic waves present. The solution is

$$\rho_L^* = \begin{cases} \rho_L H_L^{1/\gamma}, & \text{if} \quad H_L \leqslant 1 \text{ (rarefaction)}, \\ \rho_L\left[\dfrac{(\gamma+1)H_L + \gamma - 1}{(\gamma-1)H_L + \gamma + 1}\right], & \text{if} \quad H_L > 1 \text{ (shock)}, \end{cases} \tag{24}$$

and

$$\rho_R^* = \begin{cases} \rho_R H_R^{1/\gamma}, & \text{if} \quad H_R \leqslant 1 \text{ (rarefaction)}, \\ \rho_R\left[\dfrac{(\gamma+1)H_R + \gamma - 1}{(\gamma-1)H_R + \gamma + 1}\right], & \text{if} \quad H_R > 1 \text{ (shock)}. \end{cases} \tag{25}$$

(i) *Choice of wave speeds*

In implementing the WAF method, there is no ambiguity in choosing the wave speeds when the waves are contact or shock waves. For a rarefaction wave one could, in principle, choose the speed associated with the tail, the head or any ray in between them. We believe it is more appropriate, on stability grounds, to choose the speed associated with the head of the rarefaction as the representative speed of the wave. Hence the speeds λ_k are given as follows

$$\left.\begin{aligned} \lambda_1 &= \begin{cases} u_{\mathrm{L}}-a_{\mathrm{L}} & \text{if} \quad H_{\mathrm{L}} \leqslant 1, \\ u_{\mathrm{L}}-a_{\mathrm{L}}[1+((\gamma+1)/2\gamma)\,(H_{\mathrm{L}}-1)]^{\frac{1}{2}} & \text{if} \quad H_{\mathrm{L}} > 1, \end{cases} \\ \lambda_2 &= u^*, \text{ always}, \\ \lambda_3 &= \begin{cases} u_{\mathrm{R}}+a_{\mathrm{R}} & \text{if} \quad H_{\mathrm{R}} \leqslant 1, \\ u_{\mathrm{R}}+a_{\mathrm{R}}[1+((\gamma+1)/2\gamma)\,(H_{\mathrm{R}}-1)]^{\frac{1}{2}} & \text{if} \quad H_{\mathrm{R}} > 1. \end{cases} \end{aligned}\right\} \tag{26}$$

(ii) *Sonic flow*

The last case to consider is that of rarefaction waves for which the speeds associated with the head and tail have opposite signs (sonic flow). In this case the Godunov flux (6) (upwind part of the WAF method) is found by evaluating F inside the fan along the ray $x/t = 0$. For a left 'sonic' rarefaction fan the solution for u, a, ρ and p along $x/t = 0$ is

$$\left.\begin{aligned} u = (2/(\gamma+1))\,[a_{\mathrm{L}}+\tfrac{1}{2}(\gamma-1)\,u_{\mathrm{L}}], \quad a = a_{\mathrm{L}}+\tfrac{1}{2}(\gamma-1)\,(u_{\mathrm{L}}-u), \\ \rho = \rho_{\mathrm{L}}(a/a_{\mathrm{L}})^{2/(\gamma-1)}, \quad p = p_{\mathrm{L}}(\rho/\rho_{\mathrm{L}})^{\gamma}. \end{aligned}\right\} \tag{27}$$

Similarly, for a right 'sonic' rarefaction we have

$$\left.\begin{aligned} u = (2/(\gamma+1))\,[\tfrac{1}{2}(\gamma-1)\,u_{\mathrm{R}}-a_{\mathrm{R}}], \quad a = a_{\mathrm{R}}+\tfrac{1}{2}(\gamma-1)\,(u-u_{\mathrm{R}}), \\ \rho = \rho_{\mathrm{R}}(a/a_{\mathrm{R}})^{2/(\gamma-1)}, \quad p = p_{\mathrm{R}}(\rho/\rho_{\mathrm{R}})^{\gamma}. \end{aligned}\right\} \tag{28}$$

Sonic flow is tested for by using the wave speeds $u_{\mathrm{L}}-a_{\mathrm{L}}$ and $u^*-a^*_{\mathrm{L}}$ for a left rarefaction and $u_{\mathrm{R}}+a_{\mathrm{R}}$ and $u^*+a^*_{\mathrm{R}}$ for a right rarefaction, where a_{L} and a^*_{R} are the sound speeds either side of the contact discontinuity.

All the information necessary to implement the WAF method for the Euler equations (1) using an exact Riemann solver is now available to us. This can be used to compute the intercell flux $F_{i+\frac{1}{2}}$ in (12) or (15) and march in time according to (5). Application of the method as it stands will produce spurious oscillations near high gradients. The oscillation free version of the method is presented in §4.

The remaining part of this section is devoted to approximate Riemann solvers. We point out that this is not an exhaustive study on approximate Riemann solvers.

(*b*) *A two-rarefaction Riemann solver* (TR)

In the exact Riemann solver the character of the acoustic waves is not known in advance; it is part of the iterative solution procedure. These waves can be either shocks or rarefactions (see figure 2). The two-rarefaction approximation assumes that, out of the four possible wave configurations, the only one that is admissible is that in which both acoustic waves are rarefactions.

Across the left wave we have

$$a_{\mathrm{L}}^* = a_{\mathrm{L}}(p^*/p_{\mathrm{L}})^m \tag{29}$$

and

$$\tfrac{1}{2}(\gamma-1)\,u^* + a_{\mathrm{L}}^* = \tfrac{1}{2}(\gamma-1)\,u_{\mathrm{L}} + a_{\mathrm{L}}. \tag{30}$$

These equations follow from the isentropic relation and the constancy of the right Riemann invariant across the left wave. The constant m is given in (21). It follows that

$$u^* = u_{\mathrm{L}} - (2a_{\mathrm{L}}/(\gamma-1))\,[(p^*/p_{\mathrm{L}})^m - 1]. \tag{31}$$

For the right wave the corresponding equations are

$$a_{\mathrm{R}}^* = a_{\mathrm{R}}(p^*/p_{\mathrm{R}})^m, \tag{32}$$

$$\tfrac{1}{2}(\gamma-1)\,u^* - a_{\mathrm{R}}^* = \tfrac{1}{2}(\gamma-1)\,u_{\mathrm{R}} - a_{\mathrm{R}}, \tag{33}$$

$$u^* = u_{\mathrm{R}} + (2a_{\mathrm{R}}/(\gamma-1))\,[(p^*/p_{\mathrm{R}})^m - 1]. \tag{34}$$

Equations (31) and (34) give the solution for p^* and u^*, the pressure and velocity between the acoustic waves. The solution for p^* is

$$p^* = \left[\frac{a_{\mathrm{L}} + a_{\mathrm{R}} + (u_{\mathrm{L}} - u_{\mathrm{R}})\,(\gamma-1)/2}{a_{\mathrm{L}}/p_{\mathrm{L}}^m + a_{\mathrm{R}}/p_{\mathrm{R}}^m}\right]^{1/m}. \tag{35}$$

This is the value suggested as an initial value for the iteration procedure leading to the exact solution. The value for u^* may be obtained from (31) or (34).

Alternatively, one may solve (31) and (34) for u^*, instead of p^*; the result is

$$u^* = \frac{Hu_{\mathrm{L}}/a_{\mathrm{L}} + u_{\mathrm{R}}/a_{\mathrm{R}} + 2(H-1)/(\gamma-1)}{H/a_{\mathrm{L}} + 1/a_{\mathrm{R}}} \tag{36}$$

with

$$H = (p_{\mathrm{L}}/p_{\mathrm{R}})^m. \tag{37}$$

Then p^* could be obtained from (31) or (34).

(i) *Choice of wave speeds*

The wave speeds λ_1, λ_2 and λ_3 in the present approximation can be chosen as follows

$$\lambda_1 = \min\{u_{\mathrm{L}} - a_{\mathrm{L}},\quad u^* - a_{\mathrm{L}}^*\},\quad \lambda_2 = u^*,\quad \lambda_3 = \max\{u^* + a_{\mathrm{R}}^*, u_{\mathrm{R}} + a_{\mathrm{R}}\}, \tag{38}$$

where the sound speeds a_{L}^* and a_{R}^* are given by (29) and (32) respectively.

There are two more quantities to be found. These are ρ_{L}^* and ρ_{R}^*, the density either side of the contact discontinuity. One could use isentropic relations directly but since a_{L}^* and a_{R}^* are known one has

$$\rho_{\mathrm{L}}^* = \gamma p^*/a_{\mathrm{L}}^{*2},\quad \rho_{\mathrm{R}}^* = \gamma p^*/a_{\mathrm{R}}^{*2}. \tag{39}$$

Finally, the test for sonic flow is as in the previous section and the solution is as given in equations (27) or (28).

All the information needed to compute the intercell flux (12) and (13), or (14)–(16) using the TR approximation is now available.

One would expect the TR approximation to be poor for flows containing strong shocks. For flows near vacuum conditions, however, the TR approximation is remarkably good. In fact, for near-vacuum conditions generated by two rarefaction waves travelling in the opposite directions this approximation is exact.

(*c*) *A two-shock Riemann solver* (TS)

The two-shock approximation to the solution of the Riemann problem assumes *a priori* that the acoustic waves are both shock waves. This approximation does not produce a closed-form solution as does the TR approximation of the previous section, not even for gases obeying the ideal equation of state. The only advantages is that the logic in the iteration procedure to solve (18) for p^* is simplified. One uses the shock relations in (19) and (20), regardless of the value of H_L and H_R; two 'IF' statements are thus eliminated in the iteration procedure of the exact solver. This is not a significant gain, particularly if one realizes that the shock expressions require more operations. For implementations in vector machines however, the elimination of the logic can be significant.

Dukowicz (1985) introduced an approximation to the TS approximation. The iteration procedure is eliminated but complex logic is introduced to evaluate various expressions. One merit of the Dukowicz two-shock approximations is that it applies to materials with general equation of state.

(*d*) *Roe's approximate Riemann solver*

Roe's Riemann solver makes use of the fact that for linear hyperbolic systems of the form (1) the flux difference between right (R) and left states (L) can be expressed as

$$F_R^{(s)} - F_L^{(s)} = \sum_{k=1}^{N} \alpha_k \lambda_k r_k^{(s)}, \tag{40}$$

where N is the number of waves in the Riemann problem with data U_L and U_R, α_k are the wave strengths and λ_k are the respective wave speeds which here are chosen as the eigenvalues of the jacobian matrix

$$J = \partial F / \partial U. \tag{41}$$

Note that (40) is the component s associated with the flux vector in (1).

The symbol $r_k^{(s)}$ is used to denote the appropriate component of the right eigenvectors of J. Each term k in the summation (40) represents the effect of the single wave k. Note that for linear systems with constant coefficients the jacobian matrix J in (41) is constant.

Roe's approximate Riemann solver for nonlinear hyperbolic systems assumes that, locally, the jacobian matrix J, evaluated at a suitable average state, is still constant and also that the difference in states U_L, U_R (data for the local Riemann problem) satisfies

$$U_R^{(s)} - U_L^{(s)} = \sum_{k=1}^{N} \alpha_k r_k^{(s)}. \tag{42}$$

It is now a question of choosing a suitable average state to evaluate α_k, λ_k and $r_k^{(s)}$ in (40). Roe (1981) suggested the following average values for the density ρ, velocity u, enthalpy h and sound speed a

$$\tilde{\rho} = \sqrt{(\rho_L \rho_R)}, \quad \tilde{u} = (\sqrt{\rho_L}\, u_L + \sqrt{\rho_R}\, u_R)/(\sqrt{\rho_L} + \sqrt{\rho_R}) \tag{43a, b}$$

$$\tilde{h} = (\sqrt{\rho_L}\, h_L + \sqrt{\rho_R}\, h_R)/(\sqrt{\rho_L} + \sqrt{\rho_R}) \quad \tilde{a} = \{(\gamma - 1)(\tilde{h} - \tfrac{1}{2}\tilde{u}^2)\}^{\frac{1}{2}}. \tag{43c, d}$$

The specific enthalpy h in (43*c*) is

$$h = (E + p)/\rho. \tag{44}$$

In terms of the average values (43) the wave speeds λ_k become

$$\tilde{\lambda}_1 = \tilde{u}-\tilde{a}, \quad \lambda_2 = \tilde{u}, \quad \lambda_3 = \tilde{u}+\tilde{a}. \tag{45}$$

The wave strengths are

$$\tilde{\alpha}_1 = (1/2\tilde{a}^2)\,[\Delta p-\tilde{\rho}\tilde{a}\,\Delta u], \quad \tilde{\alpha}_2 = \Delta\rho-\Delta p/\tilde{a}^2, \quad \tilde{\alpha}_3 = (1/2\tilde{a}^2)\,[\Delta p+\tilde{\rho}\tilde{a}\,\Delta u]. \tag{46a–c}$$

Here $\Delta\rho = \rho_{\mathrm{R}}-\rho_{\mathrm{L}}, \Delta u = u_{\mathrm{R}}-u_{\mathrm{L}}, \Delta p = p_{\mathrm{R}}-p_{\mathrm{L}}$.

The averaged right eigenvectors are

$$R_1 = \begin{bmatrix} 1 \\ \tilde{u}-\tilde{a} \\ \tilde{h}-\tilde{u}\tilde{a} \end{bmatrix}, \quad R_2 = \begin{bmatrix} 1 \\ \tilde{u} \\ \frac{1}{2}\tilde{u}^2 \end{bmatrix}, \quad R_3 = \begin{bmatrix} 1 \\ \tilde{u}+\tilde{a} \\ \tilde{h}+\tilde{u}\tilde{a} \end{bmatrix}. \tag{47}$$

When it comes to use the Roe approximate solution of the Riemann problem in the evaluation of the intercell flux $F_{i+\frac{1}{2}}$ for the WAF method, there are at least two choices. We shall now explain each of them separately.

(e) *Re-interpretation of Roe's solver*

The approximation to the solution of the Riemann problem does not contain at least explicitly, information about the states between the acoustic waves, namely p^*, u^*, ρ_{L}^* and ρ_{R}^*. The Roe average values are not identical to the 'star' values between the acoustic waves. However, the Roe approximation can be used to obtain approximate values for the 'star' states.

The change $\Delta U^{(\mathrm{s})} = U_{\mathrm{R}}^{(\mathrm{s})} - U_{\mathrm{L}}^{(\mathrm{s})}$ for each conserved variable s is the summation of the changes across each individual wave, i.e.

$$\Delta U^{(\mathrm{s})} = \sum_{k=1}^{3} \Delta U_{i+\frac{1}{2}}^{(k)}.$$

In the Roe approximation one has $\Delta U_{i+\frac{1}{2}}^{(k,\mathrm{s})} = \alpha_k\, r_k^{(\mathrm{s})}$. Thus across the right wave the density jump is $\rho_{\mathrm{R}}-\rho_{\mathrm{R}}^* = \tilde{\alpha}_3\,\tilde{r}_3^{(1)} = \tilde{\alpha}_3$ and hence

$$\rho_{\mathrm{R}}^* = \rho_{\mathrm{R}}-\tilde{\alpha}_3. \tag{48}$$

Similarly, the value ρ_{L}^* is given by

$$\rho_{\mathrm{L}}^* = \rho_{\mathrm{L}}+\alpha_1. \tag{49}$$

To find u^* we use the jump in momentum across a single acoustic wave. Using the right wave we have

$$\rho_{\mathrm{R}}^*\,u^* = \rho_{\mathrm{R}}\,u_{\mathrm{R}}-\tilde{\alpha}_3(\tilde{u}+\tilde{a}),$$

which gives

$$u^* = (\rho_{\mathrm{R}}\,u_{\mathrm{R}}-\tilde{\alpha}_3(\tilde{u}+\tilde{a}))/\rho_{\mathrm{R}}^*.$$

If one uses the left wave then

$$u^* = (\rho_{\mathrm{L}}\,u_{\mathrm{L}}+\tilde{\alpha}_1(\tilde{u}-\tilde{a}))/\rho_{\mathrm{L}}^*.$$

For acoustic waves in which the wave strengthens $\tilde{\alpha}_1$ and $\tilde{\alpha}_3$ are very different it might be advisable to take the mean value for u^* as

$$u^* = \frac{1}{2}\left[\frac{\rho_{\mathrm{L}}\,u_{\mathrm{L}}+\tilde{\alpha}_1(\tilde{u}-\tilde{a})}{\rho_{\mathrm{L}}+\tilde{\alpha}_1}+\frac{\rho_{\mathrm{R}}\,u_{\mathrm{R}}-\tilde{\alpha}_3(\tilde{u}+\tilde{a})}{\rho_{\mathrm{R}}-\tilde{\alpha}_3}\right]. \tag{50}$$

The solution for p^* can be found from the energy equation. If one uses the right-going wave then

$$p^* = (\gamma-1)\,[E_{\mathrm{R}} - \tfrac{1}{2}\rho_{\mathrm{R}}^* u^{*2} - \tilde{\alpha}_3(\tilde{h}+\tilde{u}\tilde{a})].$$

Use of the left going wave would give another expression for p^*. As for u^*, a mean value might be more suitable for p^*, although this introduces more operations. The mean value for p^* is

$$p^* = \tfrac{1}{2}(\gamma-1)\,[E_{\mathrm{L}} + E_{\mathrm{R}} + \tilde{\alpha}_1(\tilde{h}-\tilde{u}\tilde{a}) - \tilde{\alpha}_3(\tilde{h}+\tilde{u}\tilde{a}) - \tfrac{1}{2}u^{*2}(\rho_{\mathrm{L}}^* + \rho_{\mathrm{R}}^*)]. \tag{51}$$

In this interpretation of Roe's Riemann solver one can use different wave speeds, namely

$$\lambda_1 = \min\{u_{\mathrm{L}} - a_{\mathrm{L}}, u^* - a_{\mathrm{L}}^*\}, \quad \lambda_2 = u^*, \quad \lambda_3 = \max\{u_{\mathrm{R}} + a_{\mathrm{R}}, u^* + a_{\mathrm{R}}^*\}, \tag{52a–c}$$

where the sound speeds a_{L}^* and a_{R}^* are computed from the values of equations (48), (49) and (51).

This reinterpretation of Roe's solver appears to be new and has some advantages, particularly in two dimensions.

In the original meaning of the Roe approximation to the solution of the Riemann problem the information given in (43)–(47) is used directly in (40) to produce Roe's method with intercell flux:

$$F_{i+\frac{1}{2}} = \tfrac{1}{2}(F_i + F_{i+1}) - \frac{1}{2}\sum_{k=1}^{N} \alpha_k |\lambda_k| e_k \tag{53}$$

(see Roe (1986) for details).

(f) *The Harten–Lax–van Leer Riemann solver* (HLL)

A very simple type of approximations to the solution of the Riemann problem was proposed by Harten *et al.* (1983). Their basic assumption is that the only waves present are the left and right acoustic waves. If estimates λ_1 and λ_3 for the lower and upper limits of the speeds of these acoustic waves are available then one can easily solve for the conserved variables and fluxes in the 'star' region between the acoustic waves.

Consider figure 5. Evaluation of the integral (5) in the rectangle ABCD gives

$$U_{i+\frac{1}{2}}^* = \frac{\lambda_3 U_{\mathrm{R}} - \lambda_1 U_{\mathrm{L}} - (F_{\mathrm{R}} - F_{\mathrm{L}})}{\lambda_3 - \lambda_1}, \tag{54}$$

where $U_{i+\frac{1}{2}}^*$ is the vector of conserved variables between the acoustic waves. These values can be used directly to either compute fluxes between the acoustic waves, if version (12) of WAF is to be used, or they can be used to compute a weighted average state, if version (14) of WAF is to be used. For the former version of WAF, one can also compute a 'star' flux directly as

$$F_{i+\frac{1}{2}}^* = \frac{\lambda_3 F_{\mathrm{L}} - \lambda_1 F_{\mathrm{R}} + \lambda_1 \lambda_2 (U_{\mathrm{R}} - U_{\mathrm{L}})}{\lambda_3 - \lambda_1}. \tag{55}$$

Expressions (54) and (55) are only valid for the case of figure 5, i.e. $\lambda_1 < 0$ and $\lambda_3 > 0$.

This approximate Riemann solver has one intermediate 'star' state only. That is to say, the density (temperature or internal energy) is assumed constant across the contact discontinuity. As a consequence, contact discontinuities are badly smeared.

The major problem with this Riemann solver is to find reliable and sufficiently simple estimates λ_1 and λ_3 for the lower and upper bounds for the wave speeds. Davis (1988) proposed a number of procedures for these wave-speed estimates. There is scope for the imagination in choosing the wave estimates. An important consideration in doing so is the entropy condition (see Harten (1983) and Harten *et al.* (1983) for details).

A possible choice for λ_1 and λ_3 in (54)–(55) is the wave speeds given by the Roe approximation (equation (45)), provided the entropy fix has been incorporated into the Roe scheme. On the subject of an entropy fix for the Roe solver the reader is referred to Harten & Hyman (1983).

Davis made the interesting observation that the choice

$$\lambda_3 = \Delta x/\Delta t, \quad \lambda_1 = -\lambda_3 \tag{56}$$

gives a flux $F^*_{i+\frac{1}{2}}$ associated with the Lax–Friedrich's scheme. Other obvious choices reproduce 'star' fluxes $F^*_{i+\frac{1}{2}}$ associated with familiar schemes, such as the Rusanov method (see Sod 1978).

Here we present another way of choosing estimates λ_1 and λ_3 for the wave speeds. Consider the isentropic equations of gas dynamics. This is a 2×2 system of hyperbolic equations with eigenvalues (wave speeds) $\lambda_1 = u-a$ and $\lambda_3 = u+a$. Assume that the two waves in the Riemann problem *for the isentropic equations* are rarefaction waves. Then we can find solutions for the speed u^* and the sound speed a^* between the acoustic waves. These are

$$\left.\begin{aligned} u^* &= \tfrac{1}{2}(u_{\mathrm{L}}+u_{\mathrm{R}})+(a_{\mathrm{L}}-a_{\mathrm{R}})/(\gamma-1),\\ a^* &= \tfrac{1}{2}(a_{\mathrm{L}}+a_{\mathrm{R}})+(\gamma-1)/(u_{\mathrm{L}}-u_{\mathrm{R}}). \end{aligned}\right\} \tag{57}$$

Then choose

$$\lambda_1 = \min\{u_{\mathrm{L}}-a_{\mathrm{L}}, u^*-a^*\}, \quad \lambda_3 = \max\{u_{\mathrm{R}}+a_{\mathrm{R}}, u^*+a^*\}. \tag{58}$$

Application of WAF with the HLL Riemann solver using the wave speeds (57) and (58) gives very satisfactory results. It is worth remarking that for rarefaction waves the estimates are always correct, but for shocks they may fail to bound the shock speed. A possible improvement is as follows.

Using estimates (57) and (58) and the integral form of the Euler equations (4) on the rectangle ABCD of figure 5 one obtains (54) for the conserved variables $(\rho, \rho u, E)^{\mathrm{T}}$ between the acoustic waves. Denoting the right-hand side of (54) by R one has the vector equation

$$(\rho^*, \rho^*\, u^*, E^*)^{\mathrm{T}} = (R_1, R_2, R_3)^{\mathrm{T}}. \tag{59}$$

Hence

$$\rho^* = R_1, \quad u^* = R_2/R_1, \quad p^* = (\gamma-1)\,(R_3-\tfrac{1}{2}R_2^2/R_1). \tag{60}$$

A new sound speed $a^* = (\gamma p^*/\rho^*)^{\frac{1}{2}}$ can now be computed from (60). Then we set λ_1 and λ_3 as in (58) but with revised values for u^* and a^* given by (60).

The resulting scheme (58) for choosing the wave speeds together with the modification (60) gives a very simple version of the HLL Riemann solver. Extensive numerical experiments carried out by the author (unpublished) also show that the resulting numerical methods are very robust.

The HLL Riemann solver, particularly with the proposed modification performs very well indeed for 2×2 hyperbolic systems (e.g. shallow water equations or

Figure 5

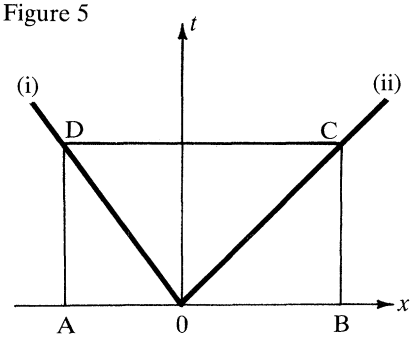

Figure 6

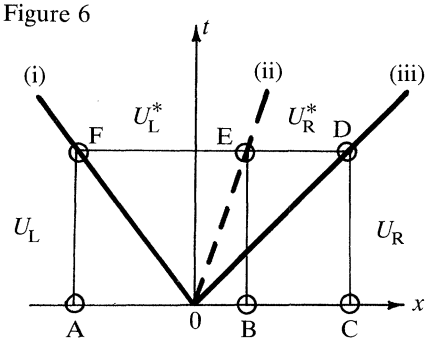

Figure 5. Simplified wave structure for the HLL approximate Riemann solver.

Figure 6. Wave configuration for the modified HLL Riemann solver with restored contact wave. (i) $\mathrm{d}x/\mathrm{d}t = \lambda_1$; (ii) $\mathrm{d}x/\mathrm{d}t = u^* = \lambda_2$; (iii) $\mathrm{d}x/\mathrm{d}t = \lambda_3$.

isentropic gas dynamics). For larger systems, however, such as the Euler equations, contact discontinuities or shear waves are ruined. One can remedy this anomaly of the HLL solver by restoring the wave associated with the contact discontinuity as follows.

Assume a wave configuration as in figure 6. Suppose we use the estimates (58) derived from equations (60). Now we have an estimate for the wave speed of the contact discontinuity, $\lambda_2 = u^*$. The integral equations (4), when evaluated on ABEF of figure 6 give

$$(\lambda_2 - \lambda_1)\, U_{\mathrm{L}}^* + (1 - \lambda_2/\lambda_3)\, F_{\mathrm{R}}^* = S, \tag{61}$$

where

$$S = \lambda_2\, U_{\mathrm{R}} - \lambda_1\, U_{\mathrm{L}} + F_{\mathrm{L}} - (\lambda_2/\lambda_3)\, F_{\mathrm{R}}. \tag{62}$$

If the integration of (4) is performed on the rectangle BCDE of figure 6 we obtain

$$(\lambda_3 - \lambda_2)\, U_{\mathrm{R}}^* - (1 - \lambda_2/\lambda_3)\, F_{\mathrm{R}}^* = Q \tag{63}$$

with

$$Q = (\lambda_3 - \lambda_2)\, U_{\mathrm{R}} - (1 - \lambda_2/\lambda_3)\, F_{\mathrm{R}}. \tag{64}$$

The reader is reminded that (61) and (63) are vector equations, where U, as in (1) stands for the vector of conserved variables $(\rho, \rho u, E)^{\mathrm{T}}$. Denote the right-hand side vectors S and Q by $(S_1, S_2, S_3)^{\mathrm{T}}$ and $(Q_1, Q_2, Q_3)^{\mathrm{T}}$ respectively, then application of (61) to the first conserved variables ρ gives

$$(\lambda_2 - \lambda_1)\, \rho_{\mathrm{L}}^* + (1 - \lambda_2/\lambda_3)\, u^* \rho_{\mathrm{R}}^* = S_1, \tag{65}$$

while (63) gives

$$(\lambda_3 - \lambda_2)\, \rho_{\mathrm{R}}^* - (1 - \lambda_2/\lambda_3)\, u^* \rho_{\mathrm{R}}^* = Q_1. \tag{66}$$

Taking $u^* = \lambda_2$ (known), (66) gives the density on the right-hand side of the contact surface as

$$\rho_{\mathrm{R}}^* = Q_1/(\lambda_3 - \lambda_2(2 - \lambda_2/\lambda_3)). \tag{67}$$

The density ρ_{L}^* on the left-hand side of the contact surface is now given by (65) and (67) as

$$\rho_{\mathrm{L}}^* = \frac{S_1}{(\lambda_2 - \lambda_1)} - \frac{(1 - \lambda_2/\lambda_3)\, \lambda_2\, Q_1}{(\lambda_2 - \lambda_1)\, [\lambda_3 - \lambda_2(2 - \lambda_2/\lambda_3)]}. \tag{68}$$

For a detailed description of a successful restoration of the contact surface for the HLL Riemann solver the reader is referred to Toro *et al.* (1992).

More on Riemann solvers for the time-dependent Euler equations can be found in Toro (1991).

4. Construction of an oscillation-free WAF

Given the second-order character of the WAF method spurious oscillations near high gradients are expected. In the original paper (Toro 1989*a*) it was demonstrated that an oscillation-free version of WAF based on the flux-limiter concept can be constructed. In this paper we present an alternative interpretation of the oscillation-free method. Strictly speaking both oscillation-free versions are mathematically equivalent, but the present formulation has some computational advantages, the resulting scheme is neater and coding is significantly simpler.

We follow Toro (1989*d*), where a detailed oscillation-free construction for a model equation was carried out. Consider the linear advection equation $u_t + au_x = 0$. Unless otherwise stated we shall assume that the constant speed a is positive. Here u is the conserved quantity and $F(u) = au$. At this stage we introduce the concept of total variation of a discrete solution $\{u_i^n\}$. The total variation of the solution at time level n, denoted by $TV(u^n)$, is defined as

$$TV(u^n) = \sum_i |u_{i+1}^n - u_i^n|. \tag{69}$$

Note that this is essentially a measure of the oscillatory character of the solution.

A large class of useful difference schemes are those whose total variation diminishes with time, i.e.

$$TV(u^{n+1}) \leqslant TV(u^n).$$

Such schemes are called *total variation diminishing schemes*, or TVD schemes for short (Harten 1983).

To apply WAF to (11) the Riemann problem for (11) must be solved. If the initial data at time level n for the local Riemann problem $RP(i, i+1)$ centred at $x_{i+\frac{1}{2}}$ is $u(t^n, x) = u_i^n$ if $x < x_{i+\frac{1}{2}}$ and $u(t^n, x) = u_{i+1}^n$ if $x > x_{i+\frac{1}{2}}$ then the solution is trivial and can be written as

$$u(x,t) = \begin{cases} u_i^n, & \text{if} \quad (x - x_{i+\frac{1}{2}})/t < a, \\ u_{i+1}^n, & \text{if} \quad (x - x_{i+\frac{1}{2}})/t > a. \end{cases} \tag{70}$$

Having solved the local Riemann problem $RP(i, i+1)$ we can now evaluate the intercell flux $F_{i+\frac{1}{2}}$. To this end it is instructive to use definition (9) for $F_{i+\frac{1}{2}}$. Since we are considering the case $a > 0$, the upwind (or upstream) region lies to the left of the characteristic line $\mathrm{d}x/\mathrm{d}t = a$ and the downwind (or downstream) region lies to the right of $\mathrm{d}x/\mathrm{d}t = a$. The respective normalized lengths associated with these regions are the weights

$$W_1 = \tfrac{1}{2}(1+\nu), \quad W_2 = \tfrac{1}{2}(1-\nu), \tag{71}$$

where $\nu = a\,\Delta t/\Delta x$ is the Courant number associated with the wave speed a.

The intercell flux $F_{i+\frac{1}{2}}$ becomes

$$F_{i+\frac{1}{2}} = \tfrac{1}{2}(1+\nu)\,au_i^n + \tfrac{1}{2}(1-\nu)\,au_{i+1}^n, \tag{72}$$

which is effectively a weighted average of the upwind and downwind parts of the solution of the local Riemann problem. Note that $W_1 + W_2 = 1$ and that $W_1, W_2 \geqslant 0$. If $W_1 = 1$ and $W_2 = 0$ the flux (72) gives the Godunov's method (first-order upwind); if

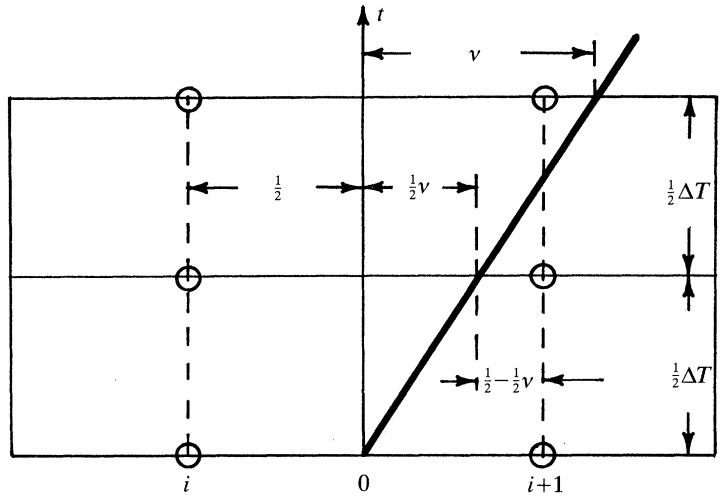

Figure 7. Illustration of the WAF intercell flux for the linear advection equation.

$W_1 = 0$ and $W_2 = 1$ the flux (72) gives a downwind method, which is unstable. The upwind method is stable but very inaccurate. If the weights in (72) are unaltered then the Lax–Wendroff method results; this is second-order accurate in space and time. In a sense the flux (72) is an average between a stable and an unstable scheme. The weight W_1 (upwind) controls stability and the weight W_2 (downwind) gives higher accuracy.

It is the inherent higher accuracy of the scheme given by (72) what produces the spurious oscillations near high gradients. In what follows we present a mechanism for eliminating the spurious oscillations.

(*a*) *Wave-speed amplifiers*

In the presence of high gradients or oscillatory data we need to reduce the role of the downwind weight W_2 and increase that of the upwind weight W_1. This can be accomplished by altering the wave speed a (see figure 7) via a function A still to be found. Generally, A will be greater than unity and thus we shall call these functions *amplifying functions* or just *amplifiers*. In constructing these functions we shall make use of the concept of total variation diminution, whereby spurious oscillations near high gradients are eliminated by introducing *artificial dissipation*. Thus the functions A are effectively numerical viscosity functions, but the process is not to be mistaken with explicit artificial viscosity methods.

Set $\bar{a} = Aa$; the modified Courant number becomes

$$\bar{\nu} = Aa\,\Delta t/\Delta x = A\nu. \tag{73}$$

The modified flux (72) becomes

$$F_{i+\frac{1}{2}} = \tfrac{1}{2}(1+\bar{\nu})\,au_i^n + \tfrac{1}{2}(1-\bar{\nu})\,au_{i+1}^n,$$

or, as in (12) with $N = 1$ for the intercell flux

$$F_{i+\frac{1}{2}} = \tfrac{1}{2}(au_i^n + au_{i+1}^n) - \tfrac{1}{2}\bar{\nu}(au_{i+1}^n - au_i^n). \tag{74}$$

To find the amplifying function A in (73) we consider first the case of positive speed a. Two obvious bounds for A are given by the fully upwinding case ($\bar{\nu} = 1$, $\overline{W}_1 = 1$,

$\overline{W}_2 = 0$) and the fully downwinding case ($\bar{\nu} = -1$, $\overline{W}_1 = 0$, $\overline{W}_2 = 1$). Thus we choose A such that

$$-\nu^{-1} \leqslant A \leqslant \nu^{-1}. \tag{75}$$

Substitution of the modified intercell fluxes $F_{i+\frac{1}{2}}$ and $F_{i-\frac{1}{2}}$ according to (74) into the conservative scheme (5) gives

$$u_i^{n+1} = u_i^n - \tfrac{1}{2}\nu\{(u_{i+1}^n - u_{i-1}^n) + \nu[A_{i+\frac{1}{2}}(u_i^n - u_{i+1}^n) - A_{i-\frac{1}{2}}(u_{i-1}^n - u_i^n)]\}. \tag{76}$$

On division through by $u_{i-1}^n - u_i^n$ and rearranging

$$\frac{u_i^{n+1} - u_i^n}{u_{i-1}^n - u_i^n} = \tfrac{1}{2}\nu^2\left[\frac{1}{r_i}\left(\frac{1}{\nu} - A_{i+\frac{1}{2}}\right) + A_{i-\frac{1}{2}} + \frac{1}{\nu}\right] \tag{77}$$

with

$$r_i = (u_i^n - u_{i-1}^n)/(u_{i+1}^n - u_i^n). \tag{78}$$

The 'flow parameter' r_i is the ratio of the upwind change to the local change in the conserved variable u.

A simple sufficient condition for avoiding overshoots or new extrema is

$$0 \leqslant (u_i^{n+1} - u_i^n)/(u_{i-1}^n - u_i^n) \leqslant 1. \tag{79}$$

That is to say, the new value u^{n+1} lies between the data values u_{i-1}^n and u_i^n. From equations (77) and (79) it follows that

$$0 \leqslant \tfrac{1}{2}\nu^2[r_i^{-1}(\nu^{-1} - A_{i+\frac{1}{2}}) + A_{i-\frac{1}{2}} + \nu^{-1}] \leqslant 1, \tag{80}$$

or

$$-\nu^{-1} \leqslant r_i^{-1}(\nu^{-1} - A_{i+\frac{1}{2}}) + A_{i-\frac{1}{2}} \leqslant (2-\nu)/\nu^2. \tag{81}$$

It is convenient to restate the constraint given by the inequalities (75) as

$$L \leqslant A_{i+\frac{1}{2}} \leqslant \nu^{-1}, \quad \text{with} \quad L \quad \text{in} \quad [-\nu^{-1}, 1]. \tag{82}$$

If $A \equiv 1$ the original scheme is unchanged. If $A > 1$ then A is strictly an amplifying function. In the analysis that follows we shall also admit the possibility of reducing the wave speed, that is to say of increasing the role of the downwind part of the scheme. The lower bound L in (82) is now open to choice within the interval $[-\nu^{-1}, 1]$.

The problem is to choose amplifiers $A_{i+\frac{1}{2}}$ so that both inequalities (81) and (82) are simultaneously satisfied. This can be achieved by taking

$$-S_{\mathrm{L}} \leqslant r_i^{-1}[\nu^{-1} - A_{i+\frac{1}{2}}] \leqslant S_{\mathrm{R}}, \tag{83}$$

$$-\nu^{-1} \leqslant L \leqslant A_{i\pm\frac{1}{2}} \leqslant \nu^{-1} \tag{84}$$

with

$$S_{\mathrm{L}} = L + 1/\nu, \quad S_{\mathrm{R}} = 2(1-\nu)/\nu^2. \tag{85}$$

The analysis leading to (83)–(85) is based on the assumption that the speed a in the model equation (12) is positive. For negative a the result is identical but ν is replaced by $|\nu|$. Hence the general case is

$$-S_{\mathrm{L}} \leqslant r_i^{-1}[|\nu|^{-1} - A_{i+\frac{1}{2}}] \leqslant S_{\mathrm{R}}, \tag{86}$$

$$-|\nu|^{-1} \leqslant L \leqslant A_{i\pm\frac{1}{2}} \leqslant |\nu|^{-1}, \tag{87}$$

with S_{L} and S_{R} redefined as

$$S_{\mathrm{L}} = L + 1/|\nu|, \quad S_{\mathrm{R}} = 2(1-|\nu|)/|\nu|^2. \tag{88}$$

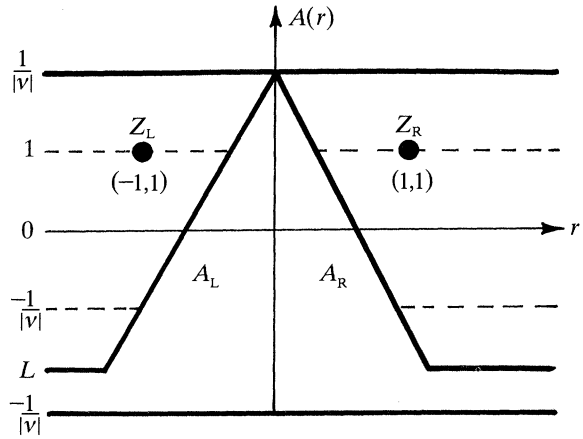

Figure 8. TVD regions in the rA-plane for WAF method as applied to the linear advection equation.

Now the main inequality (81) reads

$$-\frac{1}{|\nu|} \leqslant \frac{1}{r_i}\left[\frac{1}{|\nu|} - A_{i+\frac{1}{2}}\right] + A_{i-\frac{1}{2}} \leqslant \frac{2-|\nu|}{|\nu|^2}. \tag{89}$$

Clearly, the choices (86) and (87) satisfy (89) automatically, whose bounds we now analyse. For convenience, we ignore subscripts of the functions A and the parameter r.

From (86) $-S_{\mathrm{L}} \leqslant r^{-1}[|\nu|^{-1} - A]$. If $r > 0$, then $-S_{\mathrm{L}} r \leqslant |\nu|^{-1} - A$, or

$$A \leqslant A_{\mathrm{L}}, \quad A_{\mathrm{L}} = |\nu|^{-1} + S_{\mathrm{L}} r. \tag{90a}$$

If $r < 0$, then

$$A \geqslant A_{\mathrm{L}}. \tag{90b}$$

The upper inequality (89) gives

$$A \geqslant A_{\mathrm{R}}, \quad A_{\mathrm{R}} = |\nu|^{-1} - S_{\mathrm{R}} r, \quad \text{if} \quad r > 0, \tag{91a}$$

$$A \leqslant A_{\mathrm{R}}, \quad \text{if} \quad r < 0. \tag{91b}$$

For $L > -1/|\nu|$ in (82) there are two TVD zones Z_{L} and Z_{R} on the $r-A$ plane. These are shown in figure 8. The horizontal bounds are $A = L$ and $A = 1/|\nu|$. There are also two straight lines A_{L} and A_{R} with positive and negative slopes respectively. These lines are defined in (90a) and (91a).

The two TVD regions are, in set notation,

$$Z_{\mathrm{L}} = \{(r, A) \quad \text{such that} \quad r \leqslant 0, A \geqslant A_{\mathrm{L}}, L \leqslant A \leqslant 1/|\nu|\}, \tag{92a}$$

$$Z_{\mathrm{R}} = \{(r, A) \quad \text{such that} \quad r \geqslant 0, A \geqslant A_{\mathrm{R}}, L \leqslant A \leqslant 1/|\nu|\}. \tag{92b}$$

For the case $L = -1/|\nu|$ the zone Z_{L} coalesces to the single line $A = 1/|\nu|$. This means that if $r \leqslant 0$ only upwind differencing is allowed in this special case.

(*b*) *Construction of amplifiers A*

There are an unlimited number of choices for $A = A(r)$, where r is the flow parameter defined by (78). A simple way forward is to use the relationship that exists between our amplifiers A and flux limiters B (Sweby 1984; Roe 1986) and given by

$$A = (1 - (1 - |\nu|)B)/|\nu|. \tag{93}$$

For details see Toro (1989*d*).

There exists an enormous amount of experience in constructing and applying flux limiters B. We now profit from that experience and choose B directly to compute A in (93). A popular flux limit is the so-called MINBEE limiter with the associated $A(r)$ given as

$$A_{\mathrm{M}} = \begin{cases} 1/|\nu|, & r \leqslant 0, \\ [1-(1-|\nu|)r]/|\nu|, & 0 \leqslant r \leqslant 1, \\ 1, & r \geqslant 1. \end{cases} \tag{94}$$

In analogy with the flux limiter terminology we call the function A_{M} in (94) MINA.

Another popular flux limiter is the so-called SUPERBEE. The corresponding amplifying function, which we call SUPERA, is

$$A_S = \begin{cases} (1-2(1-|\nu|))/|\nu|, & r \geqslant 2, \\ (1-r(1-|\nu|))/|\nu| & 1 \leqslant r \leqslant 2, \\ 1, & \frac{1}{2} \leqslant r \leqslant 1, \\ (1-2r(1-|\nu|))/|\nu|, & 0 \leqslant r \leqslant \frac{1}{2}, \\ 1/|\nu|, & r \leqslant 0. \end{cases} \tag{95}$$

Alternatively, one can construct amplifiers directly. Various choices were tested by Toro (1989*d*).

Figure 9 illustrates the performance of the oscillation-free version of the method.

The most important requirement for a function A is its performance in problems other than the model equation $u_t + au_x = 0$, in particular for nonlinear systems of hyperbolic conservation laws such as the Euler equations (1). This is the subject of the next section.

(*c*) *Oscillation-free procedures for systems of equations*

The procedures described in the previous section are, strictly speaking, valid only for the model equation $u_t + au_x = 0$. For decoupled linear systems the extension is trivial. The problem arises when dealing with nonlinear systems such as the Euler equations. In this case the oscillation-free procedures are empirical.

Suppose we are solving the one-dimensional Euler equations (1). There are three waves to take care of and consequently we must construct three amplifiers A_k, one for each wave. Also, there are three fluxes, each one being affected by all three waves. Moreover, for the linear scalar case the argument r of A is itself a function of the conserved variable u (equation (78)).

Having computed A_k for each wave one then generalizes (74) to the system case as follows:

$$F_{i+\frac{1}{2}} = \tfrac{1}{2}[F_i + F_{i+1}] - \frac{1}{2}\sum_{k=1}^{N} A_k \nu_k \Delta F^{(k)}_{i+\frac{1}{2}}. \tag{96}$$

Compare the oscillation free flux (102) to the fully second-order flux (12). The modification is remarkably simple. If one chooses to use version (14)–(16) of WAF then the modified oscillation free averaged state $\bar{V}_{i+\frac{1}{2}}$ in (15) becomes

$$\bar{V}_{i+\frac{1}{2}} = \tfrac{1}{2}[V_i + V_{i+1}] - \frac{1}{2}\sum_{k=1}^{N} A_k \nu_k \Delta V^{(k)}_{i+\frac{1}{2}}. \tag{97}$$

PHILOSOPHICAL TRANSACTIONS OF THE ROYAL SOCIETY A MATHEMATICAL, PHYSICAL & ENGINEERING SCIENCES

The computation of A_k for each wave k, is based on a flow parameter $r_i^{(k)}$ defined as follows:

$$r_i^{(k)} = \begin{cases} \Delta Q^{(k)}_{i-\frac{1}{2}} / \Delta Q^{(k)}_{i+\frac{1}{2}}, & \text{if} \quad \nu_k > 0, \\ \Delta Q^{(k)}_{i+\frac{3}{2}} / \Delta Q^{(k)}_{i+\frac{1}{2}}, & \text{if} \quad \nu_k < 0, \end{cases} \tag{98}$$

where Q is a suitable flow variable. For the time-dependent Euler equations density is a good choice for Q in (98); the specific internal energy is found to be even better, but requires extra computations.

In (98) $\Delta Q^{(k)}_{i+\frac{1}{2}}$ is the jump in Q across wave k in the solution of the Riemann problem with data (U_i, U_{i+1}). We call $\Delta Q^{(k)}_{i+\frac{1}{2}}$ the local jump. The numerators in (98) are the upwind jumps in Q across the wave k. Their choice depends on the wave direction (sign of ν_k). The flow parameter $r_i^{(k)}$ in (98) is the ratio of the upwind to the local jumps in Q across the wave k.

The amplifier A_k is then simply

$$A_k = A(r_i^{(k)}), \tag{99}$$

where A is any of the amplifying functions given by equations (94) and (95).

(*d*) *An algorithm for the one-dimensional case*

Here we summarize the main steps involved in the implementation of WAF as applied to the homogeneous one-dimensional Euler equations (1).

Having specified the domain length, the number of computing cells M and the grid size Δx the following operations are performed at every time step n.

1. Solve the Riemann problem with data (U_i, U_{i+1}) and store:
   (i) the wave speeds into $WS(1,i)$, $WS(2,i)$, $WS(3,i)$;
   (ii) the ρ-jumps across each wave into $WJ(1,i)$, $WJ(2,i)$, $WJ(3,i)$;
   (iii) the star-state values p^*, u^*, ρ_{L}^* and ρ_{R}^* into $SS(k,i)$, $k = 1$ to 4.

   Here the loop runs from $i = -1$ to $M+1$.
2. Apply the CFL condition, based on true wave speeds given by the solution to local Riemann problems, to find Δt.
3. For each i, $i = 0$ to M,
   (i) compute the local Courant numbers $\nu_k = WS(k,i)\,\Delta t/\Delta x, k = 1, 3$;
   (ii) compute the amplifiers A_k, $k = 1, 2, 3$;
   (iii) modify Courant numbers $\bar{\nu}_k = A_k \nu_k$;
   (iv) compute the intercell fluxes according to (96), say. Store values into $FI(1,i)$, $FI(2,i)$, $FI(3,i)$.
4. Advance to the next time level $n+1$ using the conservative formula (5).

5. Numerical results

Here we present some numerical results for one and two-dimensional test problems.

(*a*) *Test 1: a shock-tube problem*

This very simple one-dimensional test problem has exact solution and this will be used to assess the quality of the numerical solution. This problem simulates the flow in a shock tube of unit length with a diaphragm at $x = \frac{1}{2}$ separating a left (L) and right (R) states given by

$$\rho_{\mathrm{L}} = 1.0, \quad \rho_{\mathrm{R}} = 0.125, \quad u_{\mathrm{L}} = 0, \quad u_{\mathrm{R}} = 0, \quad p_{\mathrm{L}} = 1.0, \quad p_{\mathrm{R}} = 0.1, \quad \gamma = 1.4.$$

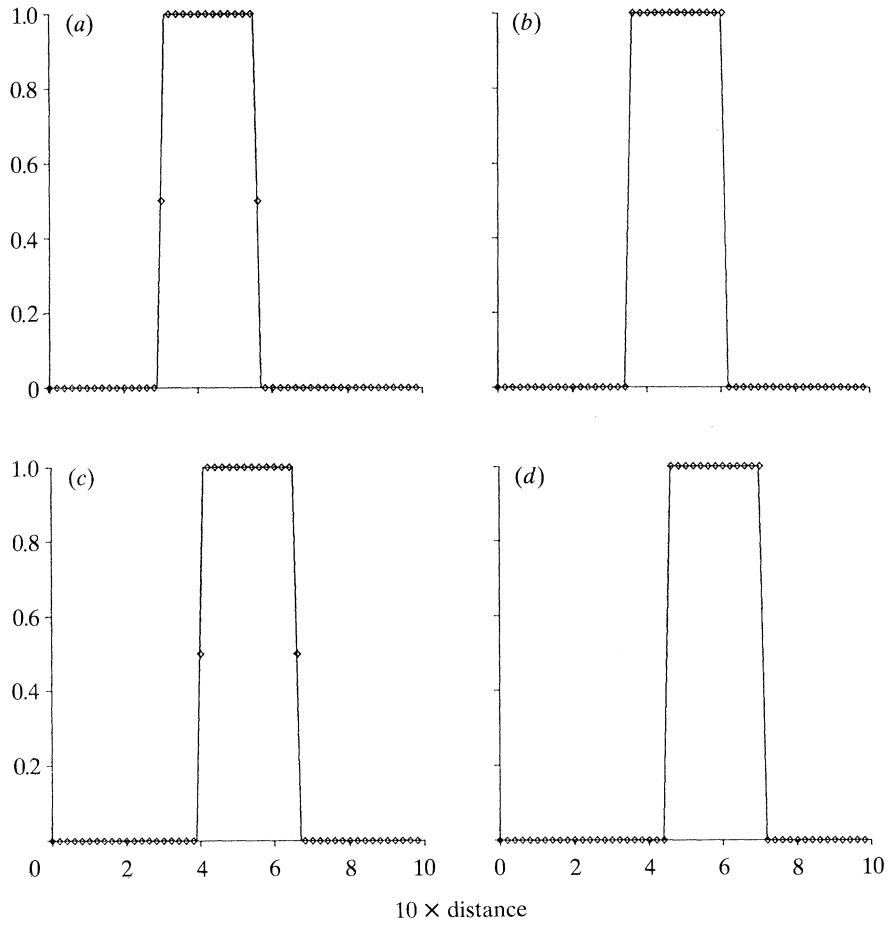

Figure 9. Comparison of the exact (line) and WAF numerical (symbol) solutions to the linear advection equation at four different times: (*a*) $t = 0.05$; (*b*) $t = 0.1$; (*c*) $t = 0.15$; (*d*) $t = 0.2$. The initial condition is a squared wave and the amplifier used is the upper limit of Z_L joined to the lower limit of Z_R in figure 8.

Results are presented in figures 10–18. The numerical solution in all cases was obtained using $M = 100$ cells and a CFL coefficient of 0.8. Results are displayed at time $t = 0.25$ units; the numerical solution is shown in symbols while the exact solution is shown by a full line.

Figure 10 shows the numerical solution obtained by using the WAF method with the exact Riemann solver and the amplifier SUPERA (equation (95)). The quantities shown are the density, pressure, particle velocity and specific internal energy. The smooth part of the flow is very accurately resolved, including the head and tail of the left-running rarefaction. The right-travelling shock wave is resolved with two interior points. This is comparable to the resolution of other RP methods such as Roe's second-order method. The contact discontinuity is resolved with three interior points, which is satisfactory. Contacts, due to their linear character, are more difficult to resolve sharply than shock waves.

Figure 11 shows the results obtained when using the Godunov's method, which is

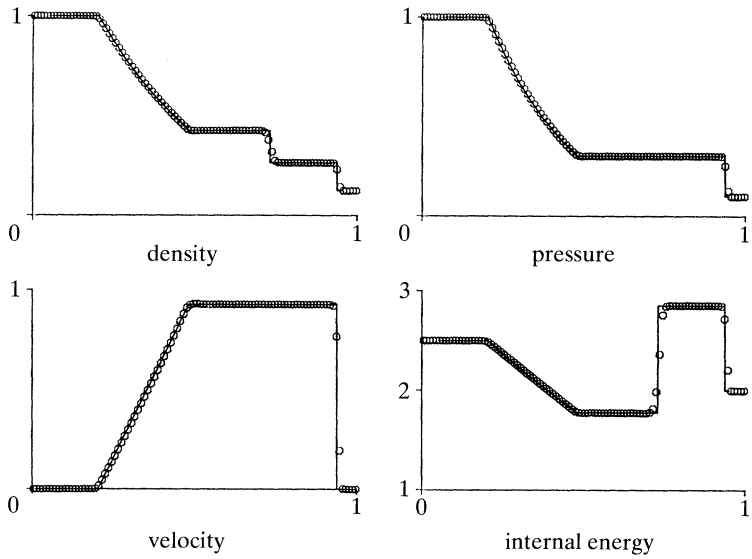

Figure 10. Comparison between the numerical (symbol) and exact (line) solutions for Test 1. The numerical results correspond to using WAF with the exact Riemann solver and SUPERA.

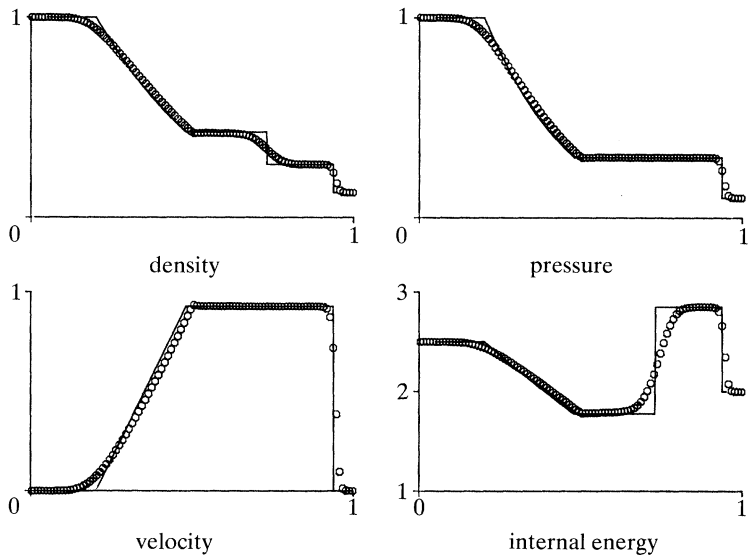

Figure 11. Comparison between the numerical (symbol) and exact (line) solutions for Test 1. The numerical results correspond to using Godunov's method with the exact Riemann solver.

only first-order accurate. The smooth parts of the solution are, as expected from a first-order method, not accurately represented. The shock wave is quite sharply resolved with about five interior points but the contact discontinuity is ruined, it has eighteen interior points. Compare figure 11 with figure 10. Such comparison is justified for two reasons. First, it illustrates the accuracy of the WAF method and second, the WAF method utilizes exactly the same Riemann problem as the Godunov's method and yet it gives much better results.

Figure 12 shows the result obtained by the fully second-order version of WAF, that

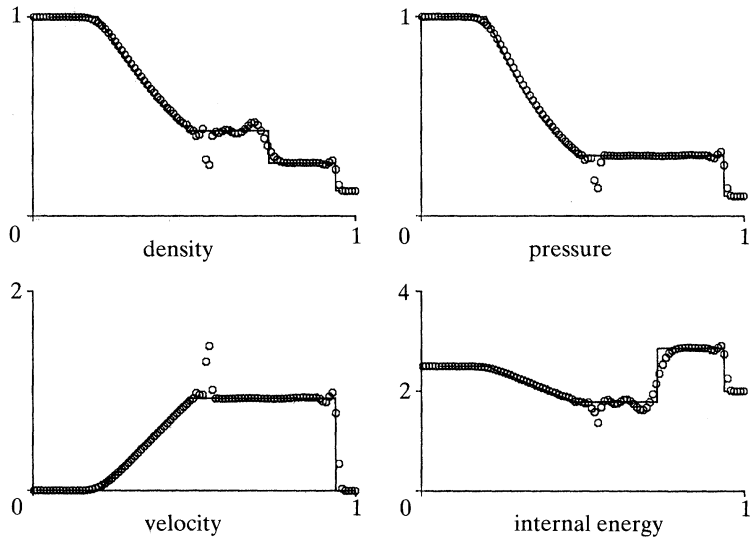

Figure 12. Comparison between the numerical (symbol) and exact (line) solutions for Test 1. The numerical results correspond to using oscillatory version of WAF ($A = 1$) together with the exact Riemann solver.

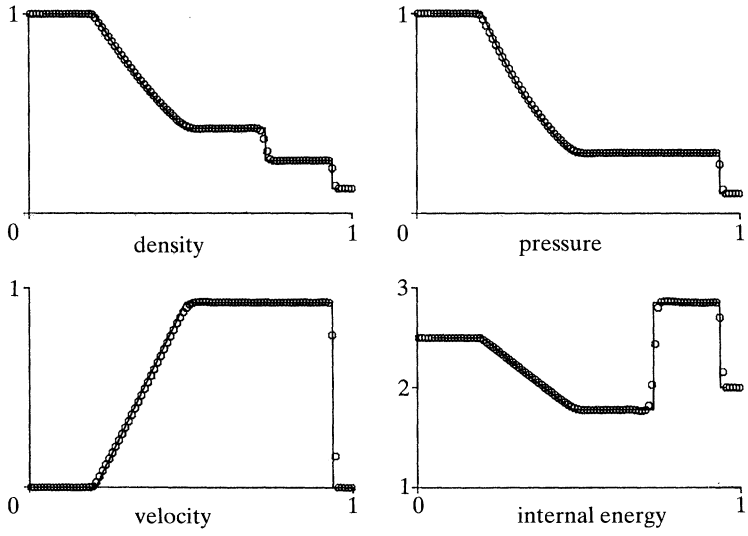

Figure 13. Comparison between the numerical (symbol) and exact (line) solutions for Test 1. Numerical results were obtained by Roe's method with the flux limiter SUPERBEE.

is when the amplifier A is identically unity. These results are very similar to those obtained by the Richtmyer–Morton method without artificial viscosity added. They are quite clearly unacceptable.

Figure 13 shows the result obtained by Roe's method. Compare with that of figure 10. The results are virtually identical. Some differences can be observed. The resolution of the tail of the rarefaction in the WAF method is slightly better; this is more apparent in the velocity and density profiles. Also, near the contact

PHILOSOPHICAL TRANSACTIONS OF THE ROYAL SOCIETY A MATHEMATICAL, PHYSICAL & ENGINEERING SCIENCES

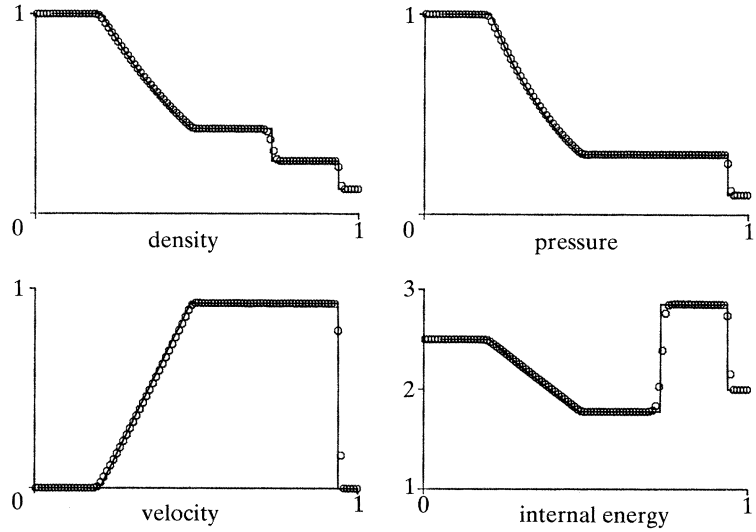

Figure 14. Comparison between the numerical (symbol) and exact (line) solutions for Test 1. The weighted-average state version of WAF with the exact Riemann solver and SUPERA is used.

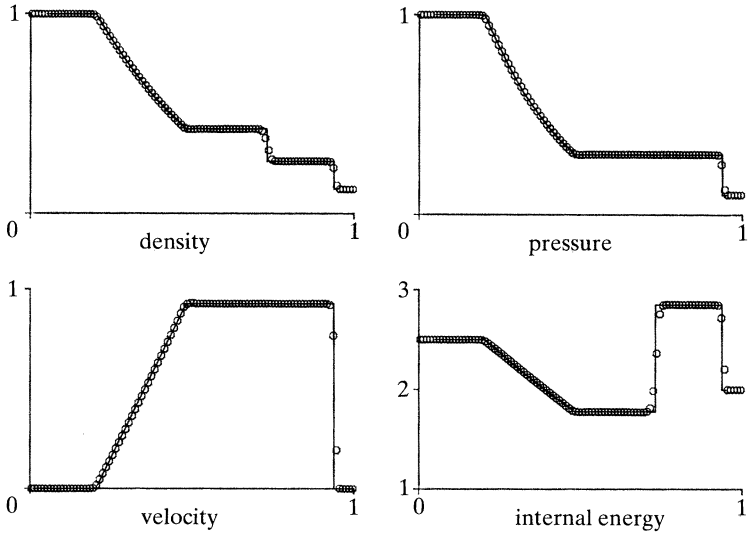

Figure 15. Comparison between the numerical (symbol) and exact (line) solutions for Test 1. WAF with the two-rarefaction approximate Riemann solver and SUPERA is used.

discontinuity Roe's method shows a slight over/under shoot, which is more clearly seen in the internal energy profile.

Figure 14 shows the results obtained by weighted-average state version of the WAF method as defined by equations (14)–(16) using the exact Riemann solver and SUPERA. These are to be compared with the results of figure 10. To plotting accuracy these are identical. At this stage, however, we are not certain whether this version is, despite its computational attractions, as robust as the weighted-average flux version (12) and (13). More numerical experimentation is required.

Figure 15 shows the WAF numerical solution using an approximate Riemann

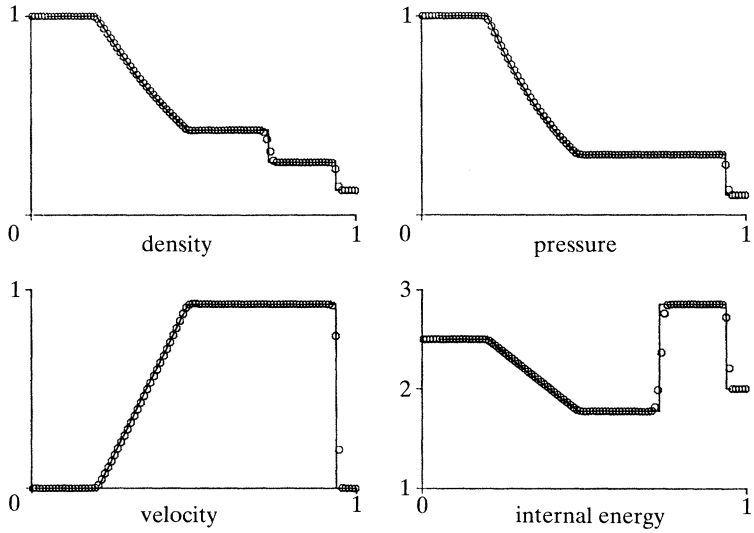

Figure 16. Comparison between the numerical (symbol) and exact (line) solutions for Test 1. WAF with the two-shock approximate Riemann solver and SUPERA is used.

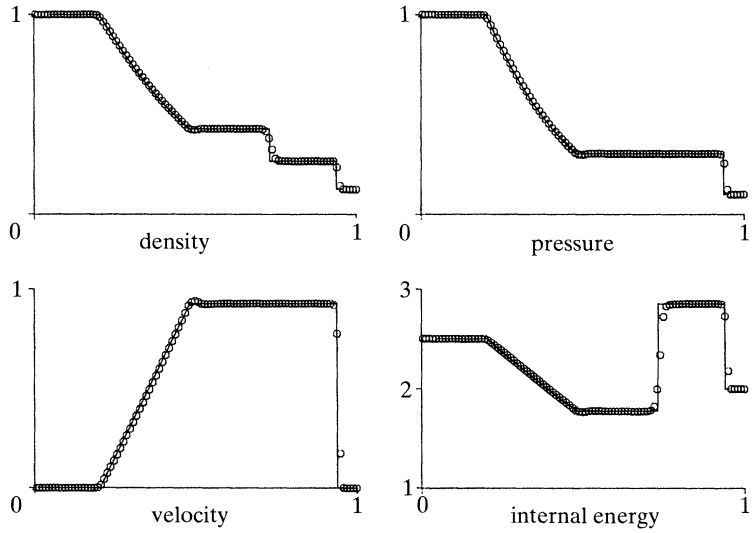

Figure 17. Comparison between the numerical (symbol) and exact (line) solutions for Test 1. WAF with the reinterpretation of Roe's approximate Riemann solver and SUPERA is used.

solver. Compare with figure 10. To plotting accuracy the results are indistinguishable. The Riemann solver used is what we called the two-rarefaction, or TR approximate Riemann solver given in §3*b*.

Figure 16 shows the WAF numerical solution when using the two-shock, or TS, approximate Riemann solver described in §3*c*. Again the numerical results, at least for this test problem, are identical to those obtained when using the exact Riemann solver.

Figure 17 shows the results from using WAF in conjunction with the reinterpretation of Roe's Riemann solver presented in §3*e*. Compare the results to those

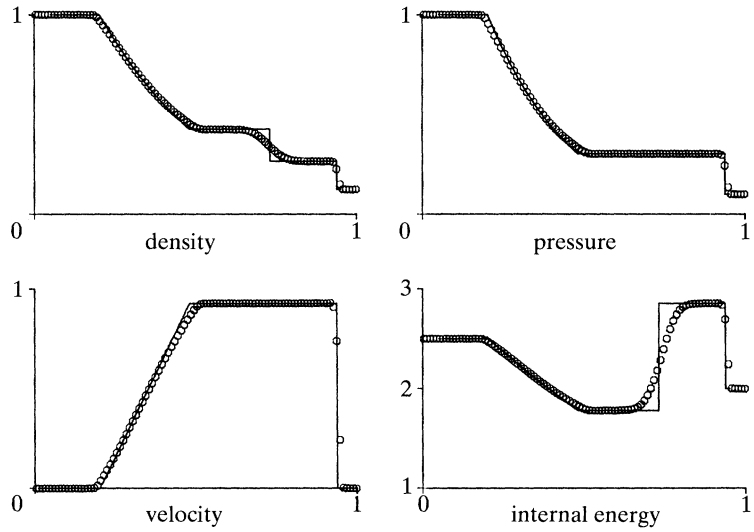

Figure 18. Comparison between the numerical (symbol) and exact (line) solutions for Test 1. WAF with the HLL and the isentropic-wave speed estimates is used. The amplifier is SUPERA.

of figure 10 (WAF with the exact Riemann solver) and to those of figure 13 (Roe's method). The resolution for all three waves is very satisfactory. There is a slight over/under shoot at the tail of the rarefaction but despite this the solution there is more accurate than that of Roe's method.

Figure 18 shows the results obtained when using the WAF method in conjunction with the Harten–Lax–van Leer, or HLL, approximate Riemann solver described in §3*f*. The two-rarefaction approximation applied to the isentropic equations is used to obtain the wave speed estimates required by the HLL solver. The isentropic estimates appear to work very well. Tests on more severe problems confirm this. As anticipated, this Riemann approximation can give accurate resolution of the acoustic waves (rarefaction and shock) but gives very poor resolution of contact discontinuities, just as first-order methods (see figure 11). Computationally, however, the simplicity of this approximate Riemann solver, especially for the wave speed estimates, has its attractions.

(*b*) *Test 2: a blast wave problem*

This one-dimensional test problem consists of a tube 5.0 m long with shock-tube data on the left and right of a diaphragm placed at $x = 0.5$ m. The initial densities, velocities and pressures are

$$\rho_{\mathrm{L}} = 1.0 \text{ kg m}^{-3}, \quad \rho_{\mathrm{R}} = 1.0 \text{ kg m}^{-3}, \quad u_{\mathrm{L}} = 0 \text{ m s}^{-1}, \quad u_{\mathrm{R}} = 0 \text{ m s}^{-1},$$

$$p_{\mathrm{L}} = 10^8 \text{ Pa}, \quad p_{\mathrm{R}} = 10^5 \text{ Pa}, \quad \gamma = 1.4.$$

The breakup of the initial discontinuity results in a shock wave travelling to the right followed by a contact discontinuity and a left-travelling rarefaction wave. The left rarefaction reflects from the left solid stationary wall and overtakes both the right travelling contact and shock. As a result the shock wave attenuates as time evolves. Problems of this kind are quite common in studying blast-wave attenuation. Figure 19 shows numerical results for density, pressure, velocity and specific internal

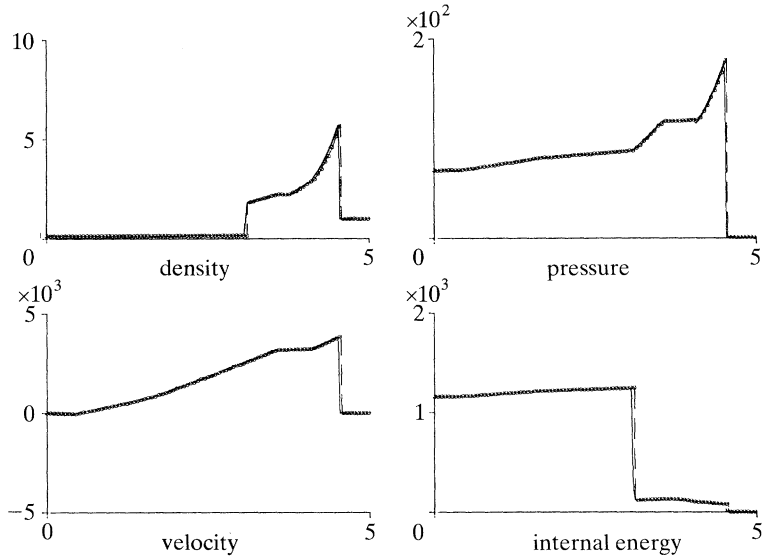

Figure 19. Comparison of numerical results for Test 2 between WAF (line) and the random choice method (symbol and dashed line).

energy at time $t = 0.65$ ms. The full-line profiles show the WAF solution using the exact Riemann solver and the amplifier SUPERA; the symbols show the solution obtained by the random choice method (RCM). For both methods we use $M = 1000$ cells with CFL coefficient of 0.8 for WAF and 0.5 for RCM. The agreement is good. A virtue of RCM is that it produces perfect discontinuities for one-dimensional problems but their positions have a random error; the random errors of RCM will also be apparent in the smooth parts of the flow as seen in figure 19. WAF on the other hand, will smear discontinuities by representing them by one to two interior points but, given its conservative character, the positions of the discontinuities are correct. Also, the representation of the smooth parts of the flow given by WAF is superior to that of RCM. However, the main advantage of WAF over RCM is manifested in multidimensional problems for which RCM does not work at all.

(c) *Test 3: a cylindrical explosion*

In this test problem we solve the time-dependent two-dimensional Euler equations on the domain $[0, 2] \times [0, 2]$ in the xy-plane. The initial conditions are those of Test 1 with $u = v = 0$; the region of high pressure and high density is the circle of radius 0.35 centred at $(1, 1)$. Cells covered partly by both sets of data are re-initialized in area-weighted fashion. The solution of the problem consists of three waves, namely an outward travelling shock followed by a contact discontinuity and rarefaction wave travelling toward the centre. Both the shock and the contact will attenuate as time evolves and the mechanism that allows this is the presence of rarefaction waves following both the contact and the shock and so the post-shock and post-contact states are not horizontal as in the one-dimensional case. Figure 20 shows the pressure distribution at time 0.3 units and figure 21 shows the density distribution at the same time. The expected symmetry of the circular waves is very well represented in the numerical solution. Both the shock and contact are sharply resolved.

Along radial distance the problem is one-dimensional with geometric source terms. Figure 22 shows a comparison between the RCM solution of the one dimensional

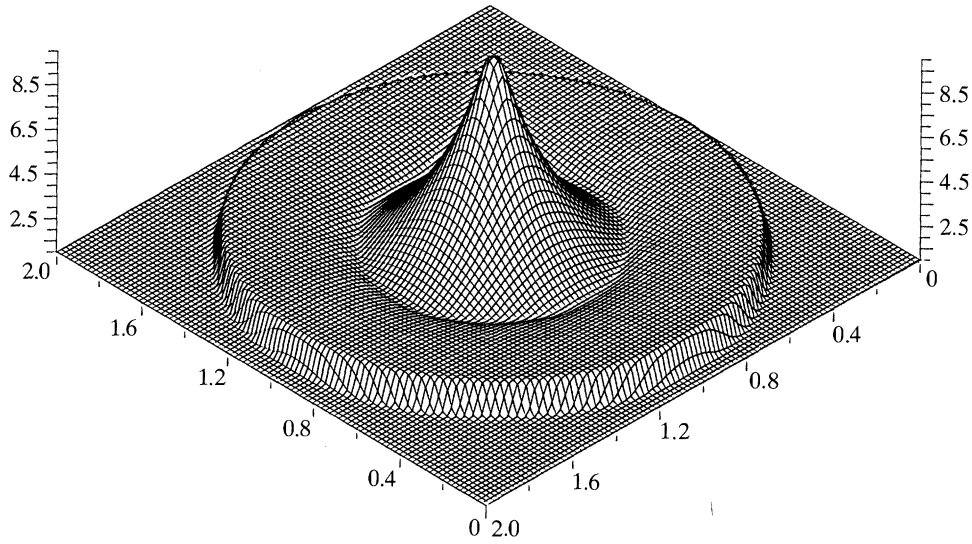

Figure 20. Computed pressure distribution for Test 3 using WAF with the two-rarefaction approximate Riemann solver and SUPERA.

problem and the WAF two-dimensional solution along one radial line. The quantities shown are pressure, density and radial velocity. For the WAF solution we have used 50 cells only while for RCM we have used 500. Good agreement is observed.

6. Conclusions

An up-to-date version of the WAF method has been presented. Significant improvements and simplifications have resulted from experience gained in applying the method to various problems. The particular features of the Euler equations, perhaps the most prominent of all hyperbolic systems, have been exploited. Several Riemann solvers that can be used with the method have also been presented. Numerical examples in one and two dimensions, to partly validate the method, show very satisfactory results. Further developments of the method of multidimensional non-cartesian geometries are currently in progress.

Appendix A. List of symbols

U	vector of conserved variables
V	vector of unknowns (e.g. conserved variables)
F	vector of fluxes in the x-direction
G	vector of fluxes in the y-direction
γ	gamma, ratio of specific heats
Δt	time-step size
Δx	spacing in x-direction
$F_{i+\frac{1}{2}}$	intercell numerical flux
λ_k	speed of wave k
ν_K	Courant number associated with
p^*	pressure in the star region in the solution of Riemann problem
u^*	particle velocity in the star region
ρ_{L}^*	density in the star region to the left of the contact
ρ_{R}^*	density in the star region to the right of the contact
a_{L}^*	sound speed in the star region to the left of the contact
a_{R}^*	sound speed in the star region to the right of the contact

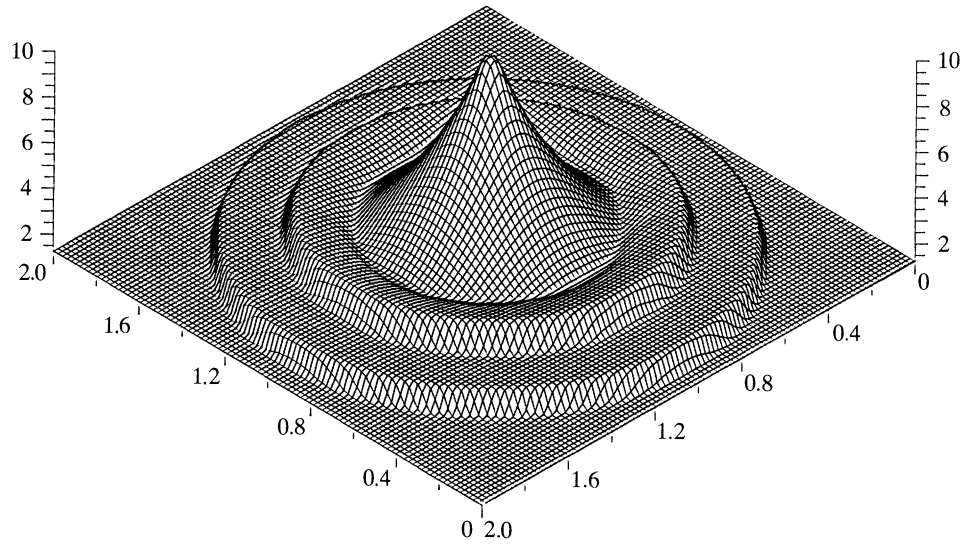

Figure 21. Computed density distribution for Test 3. Computational details as in figure 20.

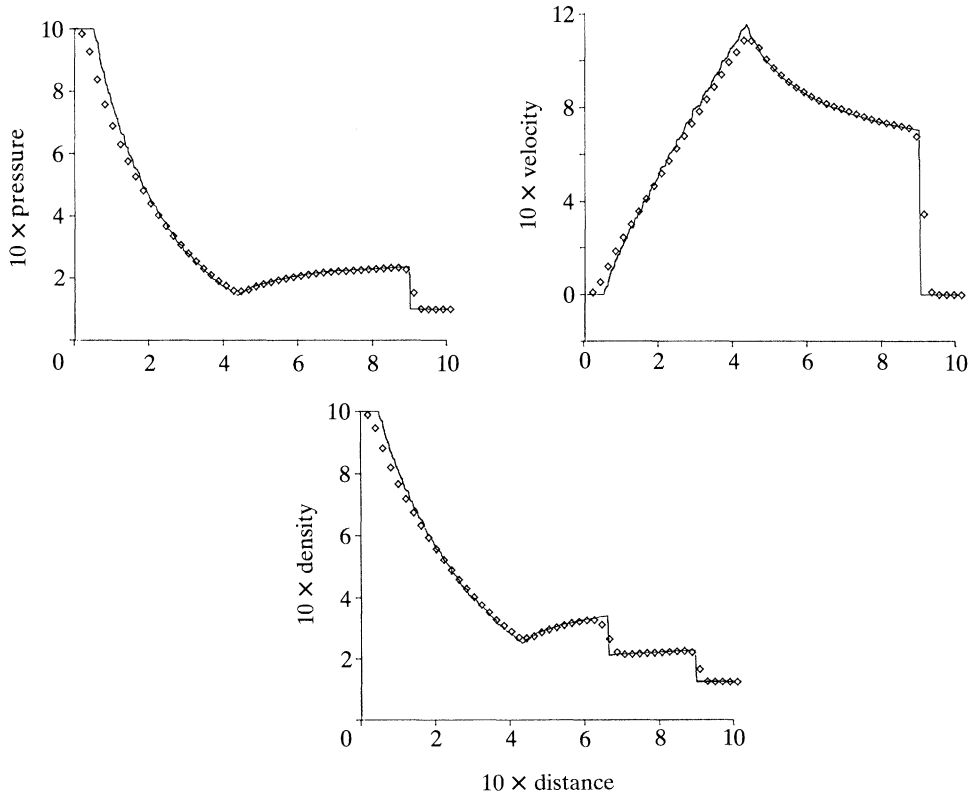

Figure 22. Comparison of numerical results for Test 3 between the two-dimensional WAF solution (symbol) and the one-dimensional random choice solution (full line). WAF uses 50 cells and RCM 500.

	wave k
ρ	density
u	x-component of velocity
v	y-component of velocity
p	pressure
a	sound speed
Z_L	left TVD region
Z_R	right TVD region
A_k	amplifier function to wave k
r_i	flow parameter to construct functions A_k
U^*	solution of Riemann problem

References

Davis, S. F. 1988 Simplified second-order Godunov-type methods. *SIAM J. Sci. statist. Comput.* **9**, 445–473.

Dukowicz, J. K. 1985 A general non-iterative Riemann solver for Godunov's method. *J. Comput. Phys.* **61**, 119–137.

Godunov, S. K. 1959 A finite difference method for the numerical computation of discontinuous solutions of the equations of fluid dynamics. *Mat. Sb.* **47**, 357–393.

Gottlieb, J. J. & Groth, C. P. T. 1988 Assessment of Riemann solvers for unsteady one-dimensional inviscid flows of perfect gases. *J. Comput. Phys.* **78**, 437–458.

Harten, A. 1983 High resolution schemes for hyperbolic conservation laws. *J. Comput. Phys.* **49**, 357–393.

Harten, A., Lax, P. D. & van Leer, B. 1983 On upstream differencing and Godunov-type schemes for hyperbolic conservation laws. *SIAM Rev.* **25**, 35–61.

Harten, A. & Hyman, J. M. 1983 Self-adjusting grid methods for hyperbolic conservation laws. *J. Comput. Phys.* **50**, 235–269.

Osher, S. 1984 Riemann solvers, the entropy condition and difference approximations. *SIAM J. numer. Analysis* **21**, 217–235.

Richtmyer, R. D. & Morton, K. W. 1967 *Difference methods for initial-value problems*, 2nd edn. New York: Interscience.

Roe, P. L. 1980 The use of the Riemann problem in finite-difference schemes. *Lecture Notes Phys.* **141**, 354–359.

Roe, P. L. 1981 Approximate Riemann solvers, parameter vectors, and difference schemes. *J. Comput. Phys.* **43**, 357–372.

Roe, P. L. 1986 Characteristic-based schemes for the Euler equations. *A. Rev. Fluid Mech.* **18**, 337–365.

Sod, G. A. 1978 A survey of several finite difference methods for system of non-linear hyperbolic conservation laws. *J. Comput. Phys.* **27**, 1–31.

Sweby, P. K. 1984 High resolution schemes using flux limiters for hyperbolic conservation laws. *SIAM J. numer. Analysis* **21**, 995–1011.

Toro, E. F. 1987 The random-choice method on a non-staggered grid utilising an efficient Riemann solver. CoA, no. 8626, Cranfield Institute of Technology, U.K.

Toro, E. F. 1989*a* A weighted average flux method for hyperbolic conservation laws. *Proc. R. Soc. Lond.* A **423**, 401–418.

Toro, E. F. 1989*b* Riemann-problem based methods for computing reactive two-phase flows. *Lecture Notes Phys.* **351**, 472–481. (*Numerical Combustion. Proc., Juan Les Pins, Antibes, France*, 1989.)

Toro, E. F. 1989*c* A fast Riemann solver with constant covolume applied to the random choice method. *Int. J. numer. Methods Fluids* **9**, 1145–1164.

Toro, E. F. 1989*d* TVD regions for the weighted average flux (WAF) method as applied to a model hyperbolic conservation law. Cranfield Report no. 8907, June 1989. College of Aeronautics, Cranfield Institute of Technology, U.K.

Toro, E. F. 1991 A linearized Riemann solver for the time-dependent Euler equations of gas dynamics. *Proc. R. Soc. Lond.* A **434**, 683–693.

Toro, E. F. 1992 Riemann problems and the WAF method for solving the two-dimensional shallow water equations. *Phil. Trans. R. Soc. Lond.* A **338**, 43–68.

PHILOSOPHICAL TRANSACTIONS OF THE ROYAL SOCIETY A MATHEMATICAL, PHYSICAL & ENGINEERING SCIENCES

Toro, E. F., Spruce, M. & Speares, W. 1992 Restoration of the contact surface in the Harten–Lax–van Leer Riemann solver. (Submitted.)

van Leer, B. 1979 Towards the ultimate conservative difference scheme. V. A second-order sequel to Godunov's method. *J. Comput. Phys.* **32**, 101–136.

Received 10 July 1991; accepted 7 April 1992

PHILOSOPHICAL TRANSACTIONS OF THE ROYAL SOCIETY A MATHEMATICAL, PHYSICAL & ENGINEERING SCIENCES